UCRL- 95597
PREPRINT

RUTILE SATURATION IN MAGMAS: IMPLICATIONS FOR Ti-Nb-Ta DEPLETION IN OROGENIC ROCK SERIES

F. J. Ryerson
E. B. Watson

This paper was prepared for submittal to
Earth and Planetary Science Letters

November 1986

DISCLAIMER

Work performed under the auspices of the U.S. Department of Energy by Lawrence Livermore National Laboratory under Contract W-7405-Eng-48.

RUTILE SATURATION IN MAGMAS: IMPLICATIONS FOR Ti–Nb–Ta DEPLETION IN OROGENIC ROCK SERIES

F. J. Ryerson

Lawrence Livermore National Laboratory

Livermore, CA 94550

E. B. Watson

Department of Geology

Rensselaer Polytechnic Institute

Troy, NY 12180–3590

Abstract

The TiO_2 contents of rutile-saturated melts ranging from basalt to rhyodacite have been investigated at P = 8–30 kb and T = 1000° – 1300°C under hydrous, CO_2-saturated, and volatile-absent conditions. Dissolved TiO_2 is positively correlated with T and not strongly dependent on P_{total}. For fixed P and T, TiO_2 content decreases markedly as the melts become more felsic. The distribution of TiO_2 between rutile and liquid, expressed as a wt% concentration ratio, D(rut/liq), is given by:

$$\ln D = -2.11 + (8615/T) + 0.014P - 0.225FM$$

where T is in Kelvins, P in Kb and FM is a melt composition parameter,

$$FM = [Na+K+2(Ca+Fe+Mg)]/Al \cdot 1/Si$$

in which the chemical symbols represent cation fractions. The first term expresses the competition of aluminate and titanate anions for charge-compensating cations, and the second term expresses the inverse dependence of dissolved TiO_2 on SiO_2 content. There is no apparent dependence of rutile solubility on water content.

For ranges of probable solidus conditions, rutile saturation in basaltic, andesitic, and dacitic liquids requires 7–9, 5–7, and 1–3 wt% TiO_2, respectively. These concentrations are well in excess of those found in the respective rock types, so depletion in Nb, Ta, and Ti and reduced Nb/Th ratios, in volcanics from collisional margins cannot be attributed to residual rutile in their source regions. Thus, Nb, Ta and Ti depletion must be an inherent property of the source region.

We suggest that the island-arc source region has been depleted in Nb and Ta by previous melt extraction (MORB). Such a process markedly depletes the LILE and HFSE

element concentrations in the residuum, but ratios such as Nb/U, Nb/Th and U/Th remain constant. The depletion of Nb relative to Th in the island-arc source occurs during hybridization of the source by rutile-saturated (Nb-depleted) melts or aqueous fluids. If a melt, it must be relatively felsic and produced under low T (900°) hydrous conditions.

Introduction

In evaluating petrogenetic models for the origin of island-arc basalts (IAB) their chemistry is typically compared to that of mid-ocean ridge basalts (MORB). This is due to the presumed similarity of their source regions. The source regions of IAB are either the subducted slab [1-6] or the overlying mantle wedge [7-9]. Variations between IAB and MORB chemistry are typically attributed to the effects of multi-stage processes including contamination by subducted sediments, mantle metasomatism by slab dehydration derived fluids and crustal contamination [9-11]. The relative contributions of these effects in individual volcanic arcs is varied and remains the subject of debate.

The major chemical differences between IAB and MORB are 1) the relative enrichment of the large ion lithophile elements (LILE), Ba, Rb, Cs, Pb, K and U, in IAB relative to MORB, and 2) the relative depletion in the high-field strength elements (HFSE), Ti, Zr, Hf, Nb and Ta, in IAB relative to MORB (Figure 1) [16-19]. The variation in HFSE concentrations between IAB and MORB is so prevalent that it forms the basis of a number of basalt classification schemes [20,21].

LILE enrichment in IAB is commonly explained in terms of processes involving slab-derived or transported material [7,17,22-24]. Such processes are also required to explain the relative enrichment of radiogenic Pb and Sr and depletion in Nd in IAB relative to MORB (cf, [11]), as well as the presence of cosmogenic ^{10}Be in IAB [25].

However, based largely upon the overlap of Sr, Nd and Pb isotopic compositions of IAB and oceanic island basalts (OIB), Morris and Hart [26] have attributed the LILE enrichment in IAB (relative to MORB) to a source component similar to that of OIB.

The depletion of HFSE, particularly Nb and Ta, in IAB (relative to both MORB and/or OIB) has been interpreted as either 1) an inherent characteristic of the IAB source region [23,27,28] or 2) due to the presence of a residual titanate phase (e.g. rutile, sphene, ilmenite, perovskite) in the IAB source region [6,26,29–31]. In the second model, the partition coefficients of Nb and Ta between titanate mineral and melt are assumed to be relatively high such that the bulk partition coefficient for these elements is greater than unity. The melt segregated from such a source region would be depleted in Nb and Ta relative to that source region. Such a mechanism could explain the depletion of HFSE in IAB produced from either a MORB or OIB source.

The validity of "residual titanate" model for HFSE depletion in IAB is dependent upon 1) the stability of titanate minerals in the appropriate melt compositions over the possible range of pressures, temperatures and volatile concentrations relevant to IAB petrogenesis, and 2) the partition coefficients of Nb and Ta between titanate minerals and IAB melts under these conditions. In this paper we present new data on rutile saturation in melt compositions ranging from basaltic to granitic over a temperature and pressure range relevant to island arc volcanism. These data, along with those from other sources, will be used to establish whether or not the "residual titanate" model is valid, and if not, what implications does its failure have to IAB petrogenesis.

General Approach

As in previous studies of accessory mineral saturation [32,33], the overall objective of this work was to determine the amount of the dissolved "essential structural constituent" (ESC) [34] necessary to saturate the melts of varying composition in the accessory mineral of interest. Rutile saturation represents the simplest of all cases in which a single oxide, TiO_2, is the sole ESC.

The study was based upon a large number of both natural and synthetic starting materials ranging from basalt to rhyolite in composition. The synthetic starting materials (TS1-TS3) are glasses modeled after natural aluminous basalts and basaltic andesite. Additional synthetic starting materials (LKA, HKA, BTC and AA) are those used previously by Watson and Harrison [33] in a study of zircon saturation.

Experimental Details

The preparation of starting materials was dependent upon both bulk composition and anticipated run composition and anticipated run conditions. The more siliceous materials, to be run at temperatures at or below 1100°, were prepared from reagent grade oxides and carbonates and were subjected to 3 fusion cycles at 1450°C. The resulting glass powder was then inspected optically to insure that no undissolved TiO_2 remained. For higher temperature experiments on basic compositions relatively large amounts of TiO_2 were added to prefused glasses to insure rutile saturation. A number of the glasses produced by subsequent fusion contained small amounts undissolved TiO_2.

Runs were made under both anhydrous and hydrous conditions. Anhydrous runs were made in graphite capsules while hydrous runs were made in sealed Au capsules initially containing 15 mg of sample and 2-15 wt% distilled H_2O. All runs were made under H_2O undersaturated conditions in a piston-cylinder apparatus. Runs at or below 18 Kbar were performed in 3/4" diameter assemblies while higher pressure runs were made in 1/2" diameter assemblies. Assemblies consisted of NaCl and Pyrex sleeves with internal filler pieces of crushable Al_2O_3, graphite, and both fired and unfired pyrophyllite. All run information is summarized in Table 1.

Results

The major-element compositions of rutile saturated melts are summarized in Table 2. Since rutile solubility will be a function of pressure, temperature and melt composition, a compositional parameter must be formulated in order to quantitatively account for compositional effects. Ideally, the activity coefficient of TiO_2 in the melt should vary systematically with this compositional parameter. The TiO_2 contents of rutile-saturated melts are presented graphically in Figure 2 as a plot of dissolved TiO_2 in the melt versus the compositional parameter, FM, where FM is given as:

$$FM = \frac{1}{Si} \cdot \frac{Na + K + 2(Ca + Mg + Fe)}{Al} \qquad (1)$$

The first term in this parameter expresses the positive dependence of the activity coefficient of TiO_2 in the melt on silica concentration. This dependence has been demonstrated by the enrichment of TiO_2 in basic liquids in coexisting basic/acidic immiscible liquid pairs [35-37]. The second term expresses the inverse dependence of the TiO_2 activity coefficient on the positive charge associated with mono- and divalent cations in excess of that required for charge compensation of tetrahedrally coordinated aluminum. This dependence has been clearly demonstrated for both zircon and rutile

solubility in the Na_2O–K_2O–Al_2O_3–SiO_2 system [38,39, respectively] in which the solubilities increased dramatically for values of $(Na_2O + K_2O)/Al_2O_3$ greater than unity. These patterns are consistent with the formation of alkali–cation high field strength element anion complexes in the melt [40]. It should be noted that in a similar study, Green and Pearson [41] concluded that alkali content decreased TiO_2 solubility for Ti–rich phases. However, in their study, SiO_2 was used as the sole compositional discriminant. As such, and in light of the data from simple systems, we prefer the formulation of FM given above.

The formulation of FM differs from that of "M", previously used to express the compositional dependence of zircon solubility [33], by the additional terms for Mg and Fe. Since the present work extends the compositional range used in the zircon solubility experiments of Watson and Harrison [33] to more basic compositions, it was felt that this modification was necessary [FM can be used as an alternative method of systematizing the zircon solubility data (in part due to the low concentrations of Fe and Mg in andesitic to granitic melts)].

In general, the rutile solubility data are very well behaved and their dependence upon melt compositions, pressure and temperature is predictable. For fixed external conditions, rutile solubility increases with increasing melt basicity as expressed by FM. For fixed values of FM, rutile solubility increases with temperature, and for fixed temperatures, there is a slight negative pressure dependence. The negative pressure dependence is best illustrated by runs conducted at 1000°C and 8 and 18 Kbar. This result is similar to that observed for apatite saturation, which also displayed a negative pressure dependence [32]. Green and Pearson [41] also observed a negative pressure dependence for Ti–rich phase solubility.

The general solubility model for rutile saturation is given as:

$$\ln D_{TiO_2}^{rutile/melt} = 2.11 + 8615/T + .014P - .225\ FM \qquad (2)$$

and provides a reasonable fit to the data (Figure 2). Since the results include those from both hydrous and anhydrous experiments, the adequacy of the model to describe the data without explicitly including the H_2O content of the melts suggests that H_2O content has little effect on rutile solubility, as previously concluded by Green and Pearson [41]. This generalization may not be extended to CO_2 concentrations, however. Two runs were conducted at 1300°C and 25 Kbar. One run was anhydrous and is in good agreement with the trends from other anhydrous experiments. The other run contained approximately 5 wt% CO_2 (added as $MgCO_3$), and contains less TiO_2 than that predicted from the trends of the anhydrous experiments. A possible explanation for this discrepancy may be that CO_2 anions in the melt [42] are competing with titanate anions for the available mono- and divalent cations. Depletion of the mono- and divalent cations available to complex with titanate anions will increase the TiO_2 activity coefficient, decreasing rutile solubility.

It should be noted that some of the more basic melts were also saturated in ilmenite. Ilmenite is less frequent as the melts become more acidic and lower in iron, thereby moving away from the ilmenite–rutile cotectic into the rutile field. This feature suggests that for basic melt compositions, relevant to island arc volcanism, the rutile solubility model may also be used to infer the stability of ilmenite. Perovskite was not present in any of these experiments, and sphene only occurred in some acidic compositions at lower temperatures.

Discussion

Rutile in IAB Source Regions

The possible occurrence of residual rutile in IAB source regions may be tested by comparing the TiO_2 contents of IAB magmas with the TiO_2 contents required for rutile saturation at the appropriate pressures and temperatures. Specifically, this method tests for the stability of rutile in the source region at the time of melt segregation. In this respect, processes occurring in or about the source region prior to melt segregation (melt or fluid metasomatism, magma or sediment mixing, diapiaric rise, etc.) are irrelevant to rutile saturation and, consequently, to Nb–Ta depletion in IAB. For instance, Brophy and Marsh (1986) have proposed that Hi–Al basalts in island arcs are produced through progressive melting of a rising diapiar originating in the subducted slab. Small degrees of partial melting within the slab produce a gravitationally unstable crystal–melt mixture which then rises diapiarically through the overlying mantle wedge. During ascent, the extent of melting increases and the residual mineralogy changes. It is quite likely that rutile will be a stable phase within quartz–eclogite subducted slab (see below). However, the partial melt generated at small degrees of melting within the slab will not be a Hi–Al basalt. Hence, the stability of rutile within the subducted slab has little relevance to Nb–Ta depletion in Hi–Al basalts. With progressive melting the partial melt composition may approach that of a Hi–Al basalt. If such a melt is segregated from its source, the question of whether or not the "eclogitic rutile" has been completely consumed is described by the solubility model.

In Figure 3 the compositions of island arc magmas from the Marianas, New Britain, Tonga–Kermadec, South Sandwich Islands, the Aleutains (see Figure caption for data sources) along with boninites from the Bonin Islands, Marianas and Cape Vogel [28] are

compared with the rutile saturation isotherms. The isotherms have been calculated for 1100°C, 200°C and 1300°C for pressures of 20 and 40 Kbar; the lower limit of each temperature field is defined by the 40 Kbar data due to the negative pressure dependence of rutile solubility. For the ranges of probable solidus conditions rutile saturation in basaltic, andesitic and dacitic liquids requires 7–9, 5–7 and 1–3 wt% TiO_2, respectively. These values are well in excess of those found in the respective rock types. Hence, rutile cannot be a residual phase during any stage of island arc volcanism. The solubility data clearly demonstrate that had rutile ever been present in the source region it must have been completely consumed prior to basaltic melt segregation.

Titanate minerals such as rutile and sphene have been observed in a number of high pressure and temperature experimental studies of basaltic bulk compositions [49–51]. Indeed, sphene and rutile are common accessory phases in basaltic amphibolites and eclogites, respectively. However, it should be emphasized that although these phases may be found in basaltic compositions, the melts with which they coexist are not basaltic. For instance, Hellman and Green [51] crystallized sphene and/or rutile from hydrous basalts at 10–25 Kbar and 700° – 1000°C. In these experiments sphene coexisted with a melt and a garnet amphibolite mineral assemblage. Although the melt composition was not analyzed in their study, it is reasonable to assume from mass balance considerations that its composition was closer to dacitic than basaltic. Results of this type cannot be used to substantiate titanate mineral–basaltic liquid equilibria.

The negative pressure dependence of rutile solubility indicates that increased pressure will tend to stabilize rutile on the liquidus of a basalt or in the residue of a basalt–producing fusion process. In principle, by invoking melt segregation at deeper levels than considered in Figure 2, rutile could be stabilized as a residual phase. Whether

or not this occurs is totally dependent upon the solidus slope of the source material. In Figure 4 the rutile solubility for values of FM spanning the range of basaltic compositions FM=7–9) has been calculated for reasonable dry peridotite solidus conditions. The results demonstrate that $d(TiO_2)/dP$ is always positive for this system. Hence, the greater the depth of melt segregation, the more difficult it becomes to saturate a eutectoid basaltic liquid with rutile.

Perovskite in IAB Source Regions

Perovskite ($CaTiO_3$) has been suggested as another possible residual titanate in the source region of IAB's [26]. A number of lines of evidence preclude this possibility. First, perovskite was not observed in any of our experiments in spite of the fact that 1) the activity of TiO_2 was fixed at its highest possible value, and 2) perovskite component was added directly to some of the compositions. However, a more general argument against perovskite stability is the activity of SiO_2 in possible IAB source regions.

If we assume a peridotite source region for IAB's, then the melts will be saturated in at least olivine and orthopyroxene at melt segregation. The coexistence of olivine and orthopyroxene buffers the activity of SiO_2 in the system by the reaction.

$$2\ Opx \rightleftharpoons Ol + SiO_2(\ell) \qquad (3)$$

Similarly, the coexistence of perovskite (Pv) and sphene (Sph) buffer the activity of SiO_2 by the reaction.

$$Sph \rightleftharpoons Pv + SiO_2(\ell) \qquad (4)$$

The positions of these buffers in terms of the activity of SiO_2 in the liquid (relative to pure molten SiO_2 at P and T) versus temperature (Figure 5) have been calculated at 1

atm, 30 Kbar and 60 Kbar using the formulation of Nicholls et al. [52]. The data displayed for the olivine–orthopyroxene reaction are those for pure enstatite and forsterite. Similar calculations using coexisting olivine and orthopyroxene compositions from high pressure and temperature experiments [53], combined with both ideal and non–ideal mixing model [54] for the crystalline phases yield virtually identical results. At each pressure, the perovskite stability field is denoted by the stippled region to the low a_{SiO_2} side of the buffer reaction. At 1 atm and 30 Kbar the chemical potential of SiO_2 in a mineral assemblage containing olivine and orthopyroxene is too high for perovskite to be stable. Perovkite would react to form sphene under these conditions. Only at 60 Kbar is perovskite stable in an assemblage containing olivine and orthopyroxene. Such pressures exceed the depth interval between the major arc complex and the Benioff zone observed in many volcanic arcs which do display Nb–Ta depletion (e.g. the Aleutians). Hence, perovskite cannot be invoked as a host phase for Nb and Ta in such arcs. Even in cases where perovskite could be stable it is expected that it would buffer the TiO_2 contents of the melts at values much greater than those found in IAB's. For instance, if the activity of TiO_2 in perovskite is only half that in rutile (an unrealistically low estimate as the chemical potentials of TiO_2 in perovskite and rutile must be equal along their cotectic), then the TiO_2 contents in the perovskite–buffered melts would be one half of that required by rutile saturation. Using the solidus slopes from Figure 4 and the reduced TiO_2 activity for perovskite yields TiO_2 saturation levels greater than 10 wt% at 50 Kbar. Such values are unrealistically high for IAB petrogenesis.

Ilmenite in IAB Source Regions

As mentioned previously, many of our experiments were saturated with ilmenite as well as rutile. This indicates that the solubility model for both phases are similar (the

caveat being that sufficient iron is available to form ilmenite). Indeed, in their experiments, Green and Pearson [41] were unable to distinguish between the saturation surfaces of a number of Ti-rich phases. This is also corroborated by the high TiO_2 contents found in lunar basaltic liquids saturated in ilmenite, typically in excess of 7 wt% TiO_2, and as high as 15 wt% TiO_2 [55,56]. These TiO_2 contents are again unrealistically high for IAB.

The similarity of rutile and ilmenite saturation surfaces may also be observed by comparing the results of "rutile-geothermometry" with those obtained from other geothermometers during low pressure fractional crystallization. In Figure 6 we have plotted the TiO_2 contents of samples from the South Shetland Islands [57] versus their bulk compositions expressed as FM. Superimposed on these data are the 1-atm rutile saturation isotherms. As fractional crystallization proceeds, (FM decreases) the TiO_2 content of the magmas first increase, then at a value FM=5 it begins to decrease. The decrease is attributed to crystallization of ilmenite and titanomagnetite. At the same point in the fractionation sequence P_2O_5 also begins to decrease, indicative of apatite fractionation. The apatite geothermometer of Harrison and Watson [58] can be used to calculate the temperatures for the apatite-saturated samples. This calculation indicates that apatite saturation occurs at approximately 975°, with the temperatures for the most fractionated samples dropping to 850°. The calculated apatite temperatures are in good agreement with those obtained from the rutile isotherms, thus demonstrating the similarity between the saturation surfaces of ilmenite-titanomagnetite and rutile.

The trace element data of Weaver et al's [57] South Shetland Island suite (SSI) can also be used to evaluate the effects of ilmenite-titanomagnetite crystallization upon Nb concentrations in the residual liquids. Using Zr concentration as a fractionation index, we

have plotted the Nb and TiO_2 concentration of the South Shetland Island Lavas (Figure 6b). At a Zr concentration of 250 ppm, TiO_2 concentrations decrease abruptly due to titanomagnetite–ilmenite crystallization. However, the Nb concentration continues to increase through the entire fractionation sequence. Therefore, the bulk partition coefficient for Nb cannot exceed unity during fractionation. The relatively constant Nb/Zr ratio (= 0.03) argues that the bulk partition coefficient for Nb remains unchanged relative to that of Zr.

The implication of the results above are that 1) $D_{Nb}^{mt\text{-}ilm/melt}$ does not greatly exceed unity and/or 2) the modal abundance of ilmenite and titanomagnetite is less than $1/D_{Nb}^{mt\text{-}ilm/melt}$. In each instance, the South Shetland Island samples represent a more favorable possibility for Nb–depletion than does peridotite melting. In the SSI suite, titanate minerals equilibrate with melts that are 1) more acidic (basaltic andesite to rhyodacite) and 2) at lower temperatures than those expected for partial melting of peridotite. Both factors would yield greater mineral–melt partition coefficients in the SSI samples than for peridotite anatexis. Further, at the onset of ilmenite and titanomagnetite fractionation in the SSI suite, TiO_2 reaches 2.5 wt%. This compares with 1200 ppm TiO_2 estimated for undepleted mantle [12]. Hence, ilmenite and titanomagnetite would be modally significant in the SSI suite relative to peridotite. Both the modal abundance of titanate minerals and their Nb mineral–melt partition coefficients are greater in basaltic liquid fractional crystallization than in peridotite anatexis. The absence of Nb depletion in basaltic liquid fractional crystallization precludes Nb depletion by residual ilmenite or titanomagnetite during peridotite anatexis.

Significance of Ti depletion in IAB

Many studies have observed that Ti is depleted in IAB relative to MORB in a manner

similar to Nb and Ta [18]. Langmuir and co-workers (personal communication) have observed that Ti in IAB is not depleted relative to the middle rare earth elements, e.g. Eu^*, and that the reduced concentrations of Ti and Eu^* in IAB may simply reflect larger degrees of melting. Nevertheless, it is worthwhile to consider the implications of Ti depletion in samples that are also depleted in Nb and Ta, as it illustrates an important rule that should be applied to all accessory mineral–melt equilibria.

For fixed external conditions the presence of an accessory phase will buffer the concentration of its essential structural constituents at their highest possible value in the coexisting melt. Conversely, the minor or trace elements which are enriched in that accessory phase will be relatively depleted in the melt. Hence, if an accessory is residual to partial melting, the concentrations of its essential structural constituents and the trace elements in which the accessory phase is enriched must display an antithetic relationship in the anatectic magma. As such, the combined depletion of both Ti and Nb–Ta in IAB is a simple argument against the presence of a residual titanate in the IAB source.

Implication for IAB Source Regions

The data and arguments presented above clearly demonstrate that the relative Nb and Ta depletion in IAB is not caused by residual titanate minerals. The high solubilities of titanate minerals in basaltic liquids preclude this alternative regardless of whether the IAB source region is in the mantle wedge or the subducted slab.

The indication that the IAB source region is depleted in Nb and Ta relative to that of MORB and OIB begs the question, "How was such a source region produced, and can it be produced from a MORB precursor?" An episode of melt extraction from a MORB–like

source region, which is then subsequently remelted to produce IAB's (e.g. a 3-stage melting model), is one possible mechanism.

In order to test the 3-stage melting model for IAB (e.g. extraction of continental crust from primitive mantle, extraction of MORB, extraction of IAB) we will compare the interelement ratios predicted by such a model with those observed in IAB's. The variations in trace element concentrations and interelement ratios in both the residuum and melts produced during partial melting of a single source are primarily dependent upon the mineral-melt partition coefficients. Since we are looking for variations relative to Nb (and Ta, which for our purposes is considered to have the same bulk partition coefficient) elements with D's both greater and less than Nb need to be considered. The relative D's for trace elements during peridotite melting can be approximated from Coryell-Masuda type diagrams [59] similar to those used by Sun et al. [14]. The commonly used placement of elements along the abscissa is that which produces a smooth abundance pattern for "N-type" MORB (Sun et al, 1979). The implicit assumptions for this ordering are that MORB is produced from the peridotitic residue of partial melting of primitive mantle and that the bulk mineral-melt partition coefficients during this event increased from left to right. As pointed out by Hofmann et al. [60] this procedure precludes the recognition of concentration anomalies relative to the normalizing composition. Any real compositional anomaly would be "erased" by the assignment of an "erroneous" partition coefficient. Using Figure 1 as a guide, the LREE are expected to have D's greater than Nb. La is an ideal choice for comparison; however, the number of volcanic rocks for which both high quality La and Nb data exist is small. The situation is slightly better for Ce, so Ce will be used for comparison although the possibility of Ce^{+4} may be a complicating factor. The alkalis, alkaline earths, U and Th are expected to have D's less than Nb. The alkalis and alkaline earths are susceptible to hydrothermal alteration, as is U, and may also be important components of slab-derived metasomatic fluids. Th appears to be the most refractory of these elements and will be used for comparison.

Ce/Nb versus Ce concentration for MORB, OIB (data from [60]) and IAB are plotted in Figure 7. The IAB data are primarily those from the New Britain arc [15] for which the Nb data were obtained by spark source mass spectrometry. The MORB–OIB data form an array in which Ce/Nb decreases with increasing Ce or, by implication, decreased degree of partial melting. Although it is widely accepted on the basis of Nd isotopic data that MORB and OIB sources have different REE patterns, the trend is generally consistent with the prediction that Ce is more compatible than Nb. It should also be noted that as the degree of partial melting increases, the ratio of incompatible elements in the melt should approach that of the source. For the least fractionated MORB (low Ce) the Ce/Nb ratio approaches a limiting value of approximately 6; this value will be used as that of the MORB source in subsequent calculations.

The IAB field does overlap that of the least fractionated MORB, and Ce/Nb shows no distinct trend with absolute Ce abundance. However, in general, the Ce/Nb ratios in IAB's are higher than those in MORB at comparable Ce concentrations, and the disparity becomes greater at higher Ce concentrations. In order to test whether repeated melt extraction from a MORB source could produce an increase in the Ce/Nb ratio we have performed a number of simple modal batch melting calculations in which a MORB source (Ce/Nb=6) was melted (F1) to produce a residue which was subsequently remelted (F2) to produce model IAB's. The results of these calculations are displayed in Figure 8 in which the Ce/Nb ratios in these melts are plotted versus the fraction of partial melting of the MORB residue (F2). The residue composition was calculated for degrees of partial melting equal to 25% and 5%, and for two values of the bulk D for Ce. The first value of D^{Ce} was calculated from the data of Frey et al. [61] for a mantle composed of 60% olivine, 20% opx, 15% cpx and 5% garnet, yielding a D = .015. In the second calculation the value of Ce was arbitrarily reduced by 50% to .008. D^{Nb} was set equal to that of U

(see discussion below) using the experimental values of Benjamin et al. [62] for cpx/melt, and Seitz and Shimizu [63] for opx/melt. Ol/melt and Gt/melt partition coefficients for U were assumed to be zero. Both models produce Ce/Nb ratios greater than those of the initial MORB source. However, in both cases the Ce/Nb ratio is primarily dependent upon the value of D^{Nb}/D^{CE}, and relatively insensitive to F1 and F2. For instance, variations in the values of F1 and F2 only cannot explain the variation in Ce/Nb for the New Britain data. Hence, although a 3-stage melting model can produce elevated Ce/Nb ratios, it is unlikely that this mechanism alone can produce the variations observed in island arcs.

Hofmann and co-workers [60,64] have demonstrated that the ratios Nb/U (47 ± 10) and Nb/Th (15.2 ± 1.7) are constant in both MORB and OIB regardless of absolute concentration. This indicates that the bulk partition coefficients for these elements during peridotite anatexis are virtually identical, and that the ratios in MORB and OIB are the same as those in their source regions. Hence, the Nb/Th and Nb/U ratios produced in both magma and residue during repeated melt extraction from a peridotite source region will remain constant. Therefore, if IAB's are produced solely by repeated melt extraction from a MORB-source, their Nb/Th must be identical to that of the MORB-OIB value. As such, these ratios place severe constraints on IAB petrogenesis.

In Figure 9 Nb/Th versus Nb for IAB's [15] are plotted along with the fields for MORB-OIB, primitive mantle and carbonaceous chondrites, and continental crust given by Hofmann et al. [60,64]. In all cases the Nb/Th ratio in IAB's is lower than that of MORB-OIB, and, with one exception, lower than that of chondrites. In many cases Nb/Th for IAB's is even lower than that for continental crust. The Nb/Th ratio for IAB's is also highly variable and shows no distinctive trend with absolute concentration. The Nb/Th ratios observed in IAB's as well as their variability cannot be explained by repeated melt extraction from a peridotite source alone.

Influence of Slab–Derived Fluids and Melts

It is clear that there is no mechanism by which simple peridotite anatexis can explain Nb anomalies in IAB's. It may be possible that metasomatic effects due to slab–derived fluids or melts, acting together with a 3–stage melting model, may reconcile these observations. With the data currently available, the potential of these effects are difficult to evaluate. However, we can place some constraints on the relative magnitudes of these effects. If we assume that 1) the IAB abundance patterns in Figure 1 are produced by melting a highly depleted and subsequently metasomatized mantle, and 2) none of the Nb has a metasomatic origin, then the relative proportion of metasomatically derived Th and U can be calculated from the Nb/U and Nb/Th ratios observed in the MORB–OIB array. The absence of Nb in slab–derived fluids is plausible, given the stability of rutile in experimentally produced basaltic eclogites (Watson and Ryerson, unpublished data). For instance, the most Nb–depleted IAB from New Britain [15] contains 0.28 ppm Nb, 0.55 ppm U and 0.11 ppm Th. The concentrations of U and Th, which could have been derived from a MORB–residue peridotite source had no metasomatism occurred are .006 ppm U and .0187 Th. Hence, 99% of the U and 83% of the Th in the source must have been metasomatically introduced. The situation is even more extreme for the Cs, Rb and Ba which are expected to be even further depleted in the unmetasomatized source. These proportions of metasomatically derived components appear to be prohibitively high, but in the absence of fluid–solid partitioning data for eclogite minerals, cannot be discounted.

Influence of Slab–Derived Melts

Slab–derived melts may also influence the Nb/Th ratios in a hybridized, depleted mantle, provided that such melts are rutile saturated at the time of melt segregation. The issues of melt production and the dynamics of melt extraction from a subducted slab

are problematical in spite of the constraints placed upon the process by experimental petrology [2,65,66]. A major controversy from which most others follow involves the thermal regime prevailing at the upper surface of a subducted slab [67]. An additional problem involves the liberation of H_2O from hydrous phases during subduction. Both issues influence the temperature, melt composition and degree of melting at any depth below the island arc. In turn, these factors control melt segregation and rutile saturation.

Given the uncertainties, the influence of slab-derived melts upon a depleted mantle source cannot be described unequivocally. However, certain end member cases can be evaluated, and a number of model-dependent constraints imposed. Brophy and Marsh [6] have described the ascent of an anhydrous partially molten diapir originating within the subducted slab. Using the experimental data of Green and Ringwood [2] they described the change in liquid composition and increasing liquid fraction during ascent. They conclude that melt extraction from such a diapir will not occur until the melt fraction reaches 0.4 at a pressure of ~33Kb and 1435°C. Using the method described by Brophy and Marsh (1986) we have calculated the liquid composition at these conditions (Table 3). The liquid contains 2.17% TiO_2; the rutile solubility model requires 11% TiO_2 for rutile saturation. Hence, the extracted liquid will not be in equilibrium with a titanate mineral, and will not impose a reduced Nb/Th ratio on the hybrid peridotite source.

At smaller degrees of melting the liquid composition in a partially molten quartz eclogite should become more felsic. This is shown by the data of Johnston [5] in which a low-K dacitic liquid (Table 3) was produced by 33% melting of an anhydrous hi-Al basalt at 1400°C, 30Kb. Rutile saturation in such a melt requires 7.06% TiO_2 which may be compared with the 1.01% the melt actually contains. This liquid clearly cannot be saturated in rutile. Hence, it is unlikely that any melt derived from an anhydrous

subducted slab would carry a Nb/Th anomaly into the overlying mantle wedge. This is largely due to the high temperature melting interval, not the inappropriateness of the melt compositions.

The addition (or retention) of water in the system reduces the temperature of the melting interval (cf. [65]). Melt compositions calculated from the mineral compositions, modal abundances, and bulk composition obtained from hydrous (5% H_2O) experiments on an olivine gabbro (Stern and Wyllie, 1978) at 900°, 1000°, 1100° and 1200° and 30Kb are given in Table 3. These conditions correspond to melt fractions of 0.2, 0.4, 0.6 and 0.8, and rutile solubilities of 0.51, 1.51, 3.72 and 7.81 wt% TiO_2. Therefore, for an average MORB with 1.51 wt% TiO_2, the partial melts produced at 900°C and 1000°C are rutile-saturated (this is true if we make the reasonable assumption that the bulk partition coefficient for TiO_2 relative to the silicate minerals is less than 1.0). If such melts can be extracted from the source, which in light of Brophy and Marsh's [6] analysis, does not appear to be unreasonable for the 1000° case, then these magmas will carry an anomalous Nb/Th signature into the overlying mantle wedge.

The Nb/Th ratio in a hybrid mantle depends upon the ratios and concentrations in the end members and the mixing proportions. Nb/Th ratios in possible mixtures are plotted versus Nb concentration in Figure 9. The residual mantle composition was calculated by assuming that average MORB (3 ppm Nb, 0.2 ppm Th) is produced by extracting a melt fraction of 0.25 from a source that contained a melt fraction of a) 0.30 and b) 0.35. In the first case, the residuum contains 15% trapped liquid, while in the second 7% trapped liquid remains. The slab-derived component was derived from melt fractions of 0.05, 0.1, 0.15 and 0.2 of a rutile-bearing MORB quartz eclogite, (modal melting with 9.85% Quartz, 29.55% Garnet, and 59.1% Cpx and 1.5% rutile). The value of $D_{Nb}^{rut/liq}$ is 30 as

recently determined by Green and Pearson [68]. The mixing lines demonstrate that the Nb/Th ratio is dominated by the slab-derived component. The influence becomes less as partial melting of the slab increases. Most importantly, the Nb/Th ratios are decreased to IAB levels with the addition of only 5-10% slab-derived liquid. Hence, the hybridization of a MORB-residual mantle with a slab-derived melt is a plausible explanation for Nb and Ta depletion in IAB's, at least in the respect that we can readily account for the abundance anomalies observed specifically for these elements. Whether the model can accommodate observed systematics for other trace elements and for Pb, Nd, and Sr isotopes is a question we will leave to individuals more expert than ourselves (and who would re-write any effort on our part, anyway).

Conclusions

The solubility of rutile in melts ranging from basaltic to rhyolitic has been determined as a function of pressure and temperature. Solubility increases with T and decreases slightly with P. Solubility increases as the melts become more basic. The rutile saturation model is given as:

$$\ln D^{\text{rutile/melt}}_{TiO_2} = 2.11 + 8615/T + .014P - .225\ FM$$

where FM is:

$$FM = \frac{1}{Si} \cdot \frac{Na + K + 2\,(Ca + Mg + Fe)}{Al}$$

Comparison of the rutile isotherms with the compositions of IAB's indicates that IAB's are not saturated in rutile at the time of melt segregation. Hence, negative Nb-Ta anomalies in IAB's, best recognized as lower Nb/Th ratios relative to MORB, cannot be the result of titanate mineral equilibria. However, under hydrous, low temperature conditions ($\leq$ 900°C), melting of the subducted slab may produce felsic liquids that are

saturated in rutile. Such melts would carry reduced Nb/Th ratios into the overlying mantle. Similarly, evolution of a rutile-saturated aqueous phase from a subducted slab may also have a reduced Nb/Th ratio. Whether or not such Nb-depleted slab-derived fluids are produced is dependent upon the thermal structure of the Benioff zone, release of fluids as a result of dehydration reactions and the dynamics of melt extraction and ascent. Mineral-vapor partition coefficients and fluid migration rates are also badly needed to evaluate these processes.

Given the present experimental data, we suggest that the source region of IAB's may be a hybrid source in which a peridotite mantle (high Nb/Th), depleted in LILE and HFSE by MORB extraction, is infiltrated by either a rutile-saturated slab-derived melt or vapor (low Nb/Th).

In the case of melt infiltration, mass-balance calculations indicate that only 5% addition of slab-derived melt will reduce the Nb/Th ratio of the hybrid source to that of IAB's. This is largely due to the extremely low concentrations of these elements in a MORB depleted peridotite. Further, the reintroduction of a low melting component to residual peridotite may ameliorate problems concerning the remelting of residual mantle. Therefore, we conclude that the role of Ti-rich phases in island-arc is not that of depleting IAB's in Nb and Ta, but rather that of preventing re-enrichment of Nb and Ta in their source region as a result of subsequent metasomatic or infiltration processes.

Two facts are worth noting in closing this discussion:

1) The success of the above model in explaining Nb and Ta abundances by no means rules out the possibility that the anomalies are produced by a more conventional (i.e., volatile phase-related) metasomatic process. As noted previously, rutile can be residual

during strictly fluid-producing events, and fluids are capable of extensive mobilization of LIL elements (Watson and Zindler, unpublished data). Distinguishing "anomalous" trace element characteristics produced by metasomatizing fluids from those produced by introduced melts is not possible with existing experimental constraints.

2) It is not only IAB that show apparent depletions in Nb and Ta. The Mesozoic Appalachian tholeiites described by Pegram [69], as well as the Proterozoic Scourie Dyke Suite described by Weaver and Tarney [70], show the same characteristic. Therefore, whatever the mechanism (or mechanisms) responsible for the depletion, it must be able to operate in circumstances more general than subduction zones alone, and is not restricted to the Phanerozoic in time.

Acknowledgements

This work was supported by the Division of Earth Sciences of the National Science Foundation, through grant no. EAR82-12453 (E.B.W.) and the Office of Basic Energy Sciences of the Department of Energy (F.J.R.). FJR would like to thank the faculty, students and staff at R.P.I. for their hospitality for the period of his visit during which time this work was undertaken. We are also grateful to A.W. Hofmann for providing us with copies of his manuscripts prior to publication, and to Charles Langmuir for providing much of our natural starting materials.

References

1. R. R. Coats, Magma type and crustal structure in the Aleutian arc. In: Crust of the Pacific Basin. Geophys. Monogr. Amer. Geophys. Union 6, 92–109, 1962.

2. T. H. Green and A. E. Ringwood, Genesis of the calc–alkaline igneous rock suite, Contrib. Mineral. Petrol. 18, 105–162, 1968.

3. B. D. Marsh and I. S. E. Carmichael, Benioff zone magmatism, J. Geophys. Res. 79, 1196–1206, 1974.

4. B. D. Marsh, The Aleutians. In: Andesites: Orogenic andesites and related rocks, R. S. Thorpe, ed., 99–114, 1982.

5. A. D. Johnston, Anydrous P–T phase relations of near primary high–alumina basalt from the South Sandwich Islands: Implications for the origin of island arcs and tonalite–trondhjemite series rocks, Contrib. Mineral. Petrol. 92, 368–382, 1986.

6. J. G. Brophy and B. D. Marsh, On the origin of Hi–Alumina arc basalt and the mechanics of melt extraction, J. Petrol., in press.

7. I. A. Nicholls and A. E. Ringwood, Effect of olivine stability in tholeiites and the production of silica saturated magmas in the island–arc environment, J. Geol. 81, 285–300, 1973.

8. J. B. Gill, Orogenic andesites and plate tectonics, Springer Verlag, 1981.

9. R. J. Arculus and R. W. Johnson, Island arc magma sources: A geochemical assessment of the roles of slab–derived components and crustal contamination, Geochem. Journal 15, 109–133, 1981.

10. A. E. Ringwood, The petrologic evolution of island arc systems, J. Geol. Soc. London 130, 183–204, 1974.

11. von Drach V., B. D. Marsh and G. J. Wasserburg, Nd and Sr isotopes in the Aleutians: multicomponent parenthood of island–arc magmas, Contrib. Mineral. Petrol. 92, 13–24, 1986.

12. E. Jagoutz, H. Palme, H. Baddenhausen, K. Blum, M. Cendales, G. Dreibus, B. Spettel, V. Lorenz and H. Wanke, The abundances of major, minor and trace elements in the earth's mantle as derived form primitive ultramafic nodules, Proc. Lunar Planet. Sci. Conf. 10th, 2031–2050, 1979.

13. D. A. Wood, J. L. Joron, M. Treuil, M. Norry and J. Tarney, Elemental and Sr isotope variations in basic lavas from Iceland and the surrounding ocean floor: the nature of mantle source inhomogeneities, Contrib. Mineral. Petrol. 70, 319–339, 1979b.

14. S. S. Sun, R. W. Nesbitt and A. V. Sharaskin, Geochemical characteristics of mid–ocean ridge basalts Earth Planet. Sci. Lett. 44, 119–138, 1979.

15. Basaltic volcanism Study Project Ch 1.2.7 Island Arc Basalts, In: Basaltic volcanism on the terrestrial planets, Pergamon Press, Inc., New York, 1286, 1981.

16. J. A. Pearce and J. R. Cann, Tectonic setting of basic volcanic rocks determined using trace element analyses, Earth Planet. Sci. Lett. 19, 290–300, 1973.

17. R. W. Kay, Geochemical constraints on the origin of Aleutian magmas. In: Island arcs, deep sea trenches and back arc basins, M. Talwani and W. C. Pittman III, ed., Amer. Geophys. Union, 229–242, 1977.

18. M. R. Perfit, D. A. Gust, A. E. Bence, R. J. Arculus and S. R. Taylor, Chemical characteristics of island–arc basalts: implications for mantle sources, Chemical Geology 30, 227–256, 1980.

19. J. A. Pearce, Trace element characteristics of lavas from destructive plate boundaries. In: Andesites: Orogenic Andesites and Related Rocks, R. S. Thorpe, ed., 525–548, 1982.

20. D. A. Wood, J. L. Joron and M. Treuil, A re–appraisal of the use of trace elements to classify and discriminate between magma series erupted in different tectonic settings, Earth Planet. Sci. Lett. 45, 326–336, 1979a.

21. J. A. Pearce and M. J. Norry, Petrogenetic implications of Ti, Zr, Y and Nb variations in volcanic rocks, Contrib. Mineral. Petrol. 69, 33–47, 1979.

22. M. R. Perfit, The petrochemistry of igneous rocks from the Cayman Trench and the Captains Bay pluton, Unalaska Island: their relation to tectonic processes at plate margins, Ph.D. Thesis, Columbia University, New York, N.Y., 273, 1977.

23. T. H. Dixon and R. Batiza, Petrology and chemistry of recent lavas in the Northern Marianas: Implications for the origin of island arc basalts, Contrib. Mineral. Petrol. 70, 167–181, 1979.

24. J. A. Whitford and P. A. Jezek, Isotopic constraints on the role of subducted sialic material in Indonesian island–arc magmatism, Geology 5, 571–575, 1982.

25. F. Tera, L. Brown, J. Morris, I. S. Sacks, J. Klein and R. Middleton, Sediment incorporation in island arc magmas: Inferences from ^{10}Be. Geochim. Cosmochim. Acta 50, 535–550, 1986.

26. J. D. Morris and S. R. Hart, Isotopic and incompatible element constraints on the genesis of island arc volcanic from Cold Bay and Amak Island, Aleutians, and implications for mantle structure, Geochim. Cosmochim. Acta 47, 2015–2030, 1983.

27. S. S. Sun and R. W. Nesbitt, Geochemical regularities and genetic significance of ophiolitic basalts, Geology 6, 689–693, 1978.

28. R. L. Hickey and F. A. Frey, Geochemical characteristics of boninite series volcanics: Implications for their source, Geochim. Cosmochim. Acta 46, 2099–2115, 1982.

29. T. H. Green, Island arc and continent–building magmatism – A review of petrogenetic models based on experimental petrology and geochemistry, Tectonophysics 63, 367–385, 1980.

30. T. H. Green, Experimental evidence for the role of accessory phases in magma genesis, J. Volc. Geotherm. Res. 10, 405–422, 1981.

31. A. D. Saunders, J. Tarney and S. D. Weaver, Transverse geochemical variations across the Antarctic Peninsula: implications for the genesis of calc–alkaline magmas, Earth Planet. Sci. Lett. 46, 344–360, 1980.

32. E. B. Watson, Apatite and phosphorus in mantle source regions: An experimental study of apatite/melt equilibria at pressures to 25 Kbar, Earth Planet. Sci. Lett. 51,322–335, 1980.

33. E. B. Watson and T. M. Harrison, Zircon saturation revisited: temperature and composition effects in a variety of crustal magma types, Earth Planet. Sci. Lett. 64, 295–304, 1983.

34. G. N. Hanson and C. H. Langmuir, Modeling of major elements in mantle–melt systems using trace element approaches, Geochim. Cosmochim. Acta 42, 725–741, 1978.

35. E. B. Watson, Two liquid partition coefficients: experimental data and geochemical implications, Contrib. Mineral. Petrol. 56, 119–134, 1976.

36. F. J. Ryerson and P. C. Hess, Implications of liquid–liquid partition coefficients to mineral–liquid partitioning, Geochim. Cosmochim. Acta 42, 921–932, 1978.

37. M. I. Wood and P. C. Hess, The structural role of Al_2O_3 and TiO_2 in immiscible silicate liquids in the system SiO_2–MgO–CaO–FeO–TiO_2–Al_2O_3, Contrib. Mineral. Petrol. 72, 319–328, 1980.

38. E. B. Watson, Zircon saturation in felsic liquids: experimental data and applications to trace element geochemistry, Contrib. Mineral. Petrol 70, 407–419, 1979.

39. J. E. Dickinson Jr. and P. C. Hess, Rutile solubility and titanium coordination in silicate melts, 49, 2289–2296, 1985.

40. F. J. Ryerson, Oxide solution mechanisms in silicate melts: Systematic variations in the activity coefficient of SiO_2, Geochim. Cosmochim. Acta 49, 637–650, 1986.

41. T. H. Green and N. J. Pearson, Ti–rich accessory phase saturation in hydrous mafic–felsic compositions at high P, T, Chem. Geol. 54, 185–201, 1986.

42. G. Fine and E. Stolper, The speciation of carbon dioxide in sodium aluminosilicate glasses, Contrib. Mineral. Petrol. 91, 105–121, 1985.

43. B. D. Marsh, Some Aleutian andesites: their nature and source, J. Geol. 84, 27–45, 1976.

44. B. D. Marsh and R. E. Leitz, Geology of Amak Island, Aleutian Islands, Alaska, J. Geol. 87, 715–723, 1979.

45. J. Kienle, S. E. Swanson and H. Pulpan, Magmatism and subduction in the eastern Aleutian Arc. In: Arc Volcanism: Physics and Tectonics, D. Shimozuru and I. Yokoyamama, ed., Terra Scientific Publishing, 1983.

46. A. Meijer and M. Reagan, Petrology and geochemistry of the Island of Sarigan in the Mariana arc; calc-alkaline volcanism in an oceanic setting, Contrib. Mineral. Petrol. 77, 337-354, 1981.

47. A. Ewart, R. N. Brothers and A. Mateen, An outline of the geology and geochemistry, and possible petrogenetic evolution of the Tonga - Kermadec - New Zealand island arc, J. Volcanol. Geotherm. Res. 2, 205-220, 1977.

48. P. E. Baker, The South Sandwich Islands: II. Petrology of the volcanic rocks, British antarctic Survey Reports 93, 34, 1978.

49. H. S. Yoder, Jr. and C. E. Tilley, Origin of basaltic magmas: An experimental study of natural and synthetic rock systems, Jour. Petrol. 3, 342-532, 1962.

50. R. N. Thompson, Melting behavior of two Snake River lavas at pressures up to 35 Kb, Carnegie Inst. Washington Yearbk. 71, 406-410, 1972.

51. P. L. Hellman and T. H. Green, The role of sphene as an accessory phase in high pressure partial melting of hydrous mafic compositions, Earth Planet. Sci. Lett. 42, 191-201, 1979.

52. J. Nicholls, I. S. E. Carmichael and J. C. Stormer, Jr., Silica activity and P_{total} in igneous rocks, Contrib. Mineral. Petrol. 33, 1-20, 1971.

53. E. Stolper, A phase diagram for Mid-ocean ridge basalts: preliminary results and implications for petrogenesis, Contrib. Mineral Petrol. 74, 13-27, 1980.

54. R. J. Williams, Reaction constants in the system $FeO-MgO-SiO_2-O_2$ at 1 atm between 900° and 1300°: experimental results, Am. J. Sci. 270, 334-360, 1971.

55. T. L. Grove and D. W. Beaty, Classification, experimental petrology and possible volcanic histories of Apollo II high-K basalts, Proc. Lunar Planet. Sci. Conf. 11th, 149-177, 1980.

56. J. W. Delano, Chemistry and liquidus phase relation of Apollo 15 red glass: Implications for the deep lunar interior, Proc. Lunar Planet. Sci. Conf. 11th, 251-288, 1980.

57. S. D. Weaver, A. D. Saunders, R. J. Pankhurst and J. Tarney, A geochemical study of magmatism associated with the initial stages of back-arc spreading, Contrib. Mineral. Petrol. 68, 151-169, 1979.

58. T. M. Harrison and E. B. Watson, The behavior of apatite during crustal anatexis: equilibrium and Kinetic considerations, Geochim. Cosmochim. Acta 48, 1467-1477, 1984.

59. C. D. Coryell, J. W. Chase and J. W. Winchester, A procedure for geochemical interpretation of terrestrial rare-earth abundance patterns, J. Geophys. Res. 68, 559-566, 1963.

60. A. W. Hofmann, K. P. Jochum, M. Seufert and W. M. White, Nb and Pb in oceanic basalts: new constraints on mantle evolution, Earth Planet. Sci. Lett., in press.

61. F. A. Frey, D. H. Green and S. D. Roy, Integrated models of basalt petrogenesis: A study of quartz tholeiites to olivine melilitites from South Eastern Australia utilizing geochemical and experimental petrological data, J. Petrol. 19, 463–513, 1978.

62. T. M. Benjamin, R. Heuser and D. S. Burnett, Solar system actinide abundances I. Laboratory partitioning between whitlockit, diopsidic clinopyroxene and anhydrous melt, abstract, In: Lunar and Planetary Science Institute, Houston, 70–77, 1978.

63. M. G. Seitz and N. Shimizu, Paritioning of uranium in the Di–Ab–An system and a spinel iherzolite system by fission track mapping, Carnegie Inst. Wash. Year Book 71, 548–553, 1972.

64. A. W. Hofmann, Nb in Hawaiian magmas: constraints on source composition and evolution, Chem. Geol. submitted.

65. C. R. Stern and P. J. Wyllie, Phase compositions through crystallization intervals in basalt–andesite–H_2O at 30 Kbar with implications for subduction zone magmas, Am. Min. 63, 641–663, 1978.

66. T. Sekine, P. J. Wyllie and D. R. Baker, Phase relationships for quartz eclogite composition in CaO–MgO–Al_2O_3–SiO_2–H_2O with implications for subduction zone magmas, Am. Min. 66, 938–950, 1981.

67. A. T. Hsui, B. D. Marsh and M. N. Toksoz, On melting of the subducted ocean crust: effects of subduction induced mantle flow, Tectonophysics 99, 207–220, 1983.

68. T. H. Green and N. J. Pearson, An experimental study of Nb and Ta partitioning between Ti–rich minerals and silicate liquids at high pressure and temperature, Geochim. Cosmochim. Acta, in press.

69. W. J. Pegram, Geochemical processes in the sub–continental mantle and the nature of crust–mantle interaction–evidence from the Mesozoic Appalachian Tholeiite Province, Ph.D. Thesis, the Massachusetts Institute of Technology, 1983.

70. B. L. Weaver and J. Tarney, the Scourie dyke suite: Petrogenesis and geochemical nature of the Proterozoic sub–continental mantle, Contrib. Mineral. Petrol. 78, 175–188, 1981.

Figure Captions

Figure 1

Comparison of mantle-normalized [12,13] abundance patterns for N-type MORB [14] and IAB from the New Britain arc [15].

Figure 2

Results of rutile solubility experiments plotted as wt% TiO_2 in the melt versus composition, FM, (see text) for pressures and temperatures as labeled. The solid lines are defined by the solubility model given as equation (2) in the text.

Figure 3

IAB compositions from a) the Aleutians [43–45], b) the New Britain [15] and Marianas arcs [46], c) the Tonga–Kermadec [47] and South Sandwich Island [48], and d) boninites from Cape Vogel [28] plotted against rutile isotherms. The stippled fields are the calculated rutile saturation concentrations at 1100°C, 1200°C and 1300°C; the upper boundary of each temperature field is defined by the 20Kb data, the lower boundary by the 40Kb data.

Figure 4

Effect of increased depth of melting of a dry peridotite upon the TiO_2 content of rutile saturated melts. Saturation values are calculated from expression (2) in the text for values of FM equal to 7 and 9, and for the solidus data given on the figure.

Figure 5

Reaction boundaries for the reactions, 1) 2 En $\rightleftharpoons$ Fo + SiO_2 (l) (dashed lines) and (2) Sph $\rightleftharpoons$ Pv + SiO_2 (l) (solid lines) in terms of the activity of SiO_2 in the melt versus temperature (En = enstatite, Fo = forsterite, Sph = sphene, Pv = perovskite). The stippled region shows the side of the reaction (2) for which perovskite is stable. Reaction boundaries were calculated from the data of Nicholls et al. [52].

Figure 6

a) TiO_2 vs FM for lavas from the Scotia Arc [57] plotted against 1-atm rutile isotherms. The solid symbols denote samples saturated in both ilmenite-magnetite and apatite. The "apatite-temperatures" (see text) range from 975° at FM > 5 and 850°C at FM < 3, and are coincident with the rutile isotherms. b) Nb (left axis, open symbol) and TiO_2 (right axis, filled symbols) versus Zr for the lavas in Figure 6b [57].

Figure 7

a) Ce/Nb vs Ce for MORB and OIB [60] and IAB's from the New Britain Arc [15]. b) Nb/Th vs Nb for MORB and OIB [60,64] and IAB's from the New Britain Arc [15].

Figure 8

Variation in Ce/Nb ratios in magmas produced by melting the peridotitic residuum to MORB extraction. The residual peridotite composition is calculated for the extraction of MORB melt fractions (F1) or .05 and .25, and for bulk partition coefficients for Nb equal to 0.002, and for Ce equal to 0.015 and 0.008. The Ce/Nb ratios in the magmas are plotted versus the melt fraction extracted (F2) during the subsequent remelting of the residual peridotite.

Figure 9

Variation in Nb/Th versus Nb for mixtures of depleted peridotite plus trapped melt and a slab derived melt. Peridotite plus trapped melt end members are: "A" 25% melt extracted from a source with 35% melt, and "B" 25% melt extracted from a source with 30% melt. The slab component is calculated for melt fractions of .05 and .02. Data from the New Britain arc are shown as solid symbols.

TABLE 1

Run No.	Starting Mtl	T°C	P(Kb)	H_2O	Results[a]
T1	BCR-1 (G)[b]	1250	15	0	
T4	Ex 136 (G)	1250	15	0	
T5	Paricutin (G)	1250	15	0	
T8	BCR-1 (G)	1180	15	0	pc,ilm
T9	Ex 136 (G)	1180	15	0	
T10	Paricutin (G)	1180	15	0	pc,cpx
T12	BCR-1 (Au)[c]	1100	18	6.9	cpx
T17	TS2 (Au)	1130	18	2	cpx
T23	Ex 136 (G)	1150	10	0	cpx,zir
T31	TS2 (G)	1300	25	0	gt,cpx,pc,q
T32	TS3 (G)	1300	25	0	gt,cpx,pc,q
T33	TS1 (G)	1350	25	0	cpx,pc
T34	TS2 (G)	1350	25	0	cpx,pc
T35	TS3 (G)	1350	25	0	
T39	TS1 (G)	1350	30	0	cpx,pc,q,2gl
T40	TS2 (G)	1350	30	0	cpx,q,2gl
T41	TS3 (G)	1350	30	0	cpx,gt
T44	Ex 136 (G)	1365	25	0	ru
T50	TS2 (Pt/C)[d]	1300	25	10% $MgCO_3$	cpx
T51	TS1* (Au)	1000	18	12.9	
T52	TS2* (Au)	1000	18	13.8	
T53	TS3* (Au)	1000	18	11.05	cpx,ilm
T54	AA (Au)	1000	18	13.6	
T55	LKA (Au)	1000	18	11.5	
T56	HKA (Au)	1000	18	12.5	
R6	HKA (Au)	1000	8	6	sph
R7	LKA (Au)	1000	8	6	
R8	AA (Au)	1000	8	6	
R9	BTC (Au)	1000	8	6	
R10	LCO (Au)	1000	8	6	

a. Phases present in addition to rutile and glass
b. Graphite capsule
c. Au capsule
d. Graphite inner capsule, Pt outer capsule.

*Crystalline rutile added

SP8: Cortlandt Alkali Basalt Glass
Ex 136: Exeter 136 Andesite

TABLE 2

	T52 (5)[a]	T53 (5)	T54 (5)	T55 (5)	T56 (5)	T58 (9)
SiO_2	50.63 (.56)	54.85 (.58)	52.77 (.47)	53.67 (.31)	56.12 (.46)	63.67 (.57)
TiO_2	1.94 (.14)	.74 (.22)	1.76 (.12)	1.67 (.19)	1.55 (.23)	2.21 (.17)
Al_2O_3	16.60 (.27)	20.45 (.49)	15.70 (.21)	15.02 (.18)	15.48 (.37)	18.11 (.60)
FeO	3.95 (.22)	1.42 (.44)	3.34 (.36)	3.14 (.21)	2.27 (.27)	4.72 (.22)
MnO	–	–	–	–	–	–
MgO	2.96 (.33)	.22 (.24)	1.79 (.30)	2.10 (.29)	1.31 (.41)	1.62 (.15)
CaO	9.05 (.27)	6.38 (.20)	7.99 (.29)	6.21 (.28)	5.45 (.23)	3.16 (.10)
Na_2O	3.10[b]	3.39 (.19)	2.30[b]	3.30[b]	3.60[b]	2.02 (.07)
K_2O	.52 (.12)	.69 (.09)	1.02 (.13)	1.88 (.18)	2.94 (.05)	4.47 (.14)
Total	88.75	88.14	86.67	86.99	88.72	99.97
FM	4.01	1.74	3.2	3.32	2.82	2.72

	T59 (7)	R6[c]	R7[c]	R8 (8)	R9 (9)	R10
SiO_2	60.78 (1.10)	56.08	55.05	52.89 (.34)	58.42 (.78)	68.38 (.88)
TiO_2	2.79 (.31)	1.82	1.88	2.17 (.11)	1.29 (.15)	1.03 (.12)
Al_2O_3	17.85 (.51)	16.37	16.60	17.15 (.21)	18.29 (.42)	12.12 (.12)
FeO	3.55 (.12)	3.38	3.78	4.33 (.14)	3.36 (.13)	.59 (.28)
MnO	–	–	–	–	–	–
MgO	1.62 (.03)	1.49	2.05	2.18 (.07)	1.36 (.03)	.10 (.02)
CaO	5.68 (.12)	4.80	6.47	8.20 (.12)	2.64 (.07)	.53 (.03)
Na_2O	4.15 (.09)	3.57	3.29	2.53 (.10)	1.90 (.14)	2.93 (.42)
K_2O	3.16 (.07)	2.94	1.50	.61 (.04)	3.58 (.13)	4.26 (.10)
Total	99.58	90.37	90.62	90.06	90.78	90.02
FM	2.94	2.80	3.13	3.32	1.81	1.33

a. Number of analyses.
b. Na_2O volatilized during analysis, calculated from mass balance.
c. Only one analysis obtained

	T1 (5)	T4 (5)	T5 (5)	T8 (5)	T9 (5)	T10 (5)
SiO_2	52.20 (.11)	54.37 (.28)	52.72 (.38)	51.88 (.70)	54.78 (.37)	54.03 (.25)
TiO_2	8.94 (.26)	7.20 (.18)	7.58 (.17)	7.34 (.22)	5.37 (.33)	6.41 (.14)
Al_2O_3	12.58 (.12)	14.88 (.08)	16.11 (.07)	12.79 (.16)	15.05 (.12)	13.66 (.13)
FeO	11.38 (.12)	6.39 (.11)	6.60 (.10)	11.96 (.46)	6.46 (.11)	9.69 (.14)
MnO	–	–	–	–	–	–
MgO	3.14 (.06)	4.51 (.07)	4.71 (.03)	3.70 (.11)	4.46 (.07)	3.62 (.11)
CaO	6.41 (.04)	5.92 (.03)	6.31 (.05)	6.91 (.18)	6.08 (.09)	6.10 (.19)
Na_2O	2.98 (.09)	2.94 (.23)	3.96 (.16)	3.02 (.13)	3.10 (.11)	3.40 (.18)
K_2O	1.69 (.04)	2.07 (.03)	1.16 (.04)	1.54 (.10)	2.10 (.05)	1.92 (.07)
Total	99.32	98.28	98.95	99.14	97.40	98.83
FM	6.65	4.93	4.99	7.08	4.9	5.87

	T12 (5)	T17 (6)	T23 (5)	T31 (4)	T32 (4)
SiO_2	61.98 (.42)	53.52 (.26)	55.85 (.48)	57.49 (.75)	54.25 (1.31)
TiO_2	2.31 (.49)	3.39 (.06)	4.40 (.13)	5.67 (.11)	5.18 (.75)
Al_2O_3	14.65 (.17)	18.13 (.06)	16.02 (.10)	17.25 (.19)	17.01 (.40)
FeO	6.39 (.22)	3.88 (.02)	6.16 (.19)	6.42 (.11)	7.06 (.49)
MnO	-	-	-	–	–
MgO	.76 (.02)	3.52 (.07)	3.91 (.10)	2.48 (.35)	3.16 (1.09)
CaO	3.40 (.14)	8.16 (.07)	6.17 (.12)	7.75 (.14)	7.50 (1.20)
Na_2O	3.25 (.19)		3.21 (.12)	1.11 (.06)	2.90 (.70)
K_2O	3.22 (.11)	0.56 (.01)	2.26 (.05)	2.62 (.13)	1.17 (.34)
Total	95.96	94.44	97.98	100.77	98.23
FM	2.91	3.7	4.4	3.61	4.25

	T33 (7)	T34 (6)	T35 (7)	T39	T40 (6)	T41 (5)
SiO_2	52.81 (.72)	50.38 (.64)	47.32 (.43)	60.37 (.81)	59.19 (1.03)	56.49 (.26)
TiO_2	6.84 (.21)	8.19 (.25)	9.33 (.14)	4.95 (.28)	5.54 (.13)	5.99 (.16)
Al_2O_3	18.53 (.38)	18.22 (.27)	17.60 (.33)	18.47 (.44)	17.95 (.15)	17.16 (.06)
FeO	3.88 (.14)	4.85 (.12)	5.78 (.11)	4.63 (.30)	5.36 (.19)	6.27 (.15)
MnO	0.01 (.01)	–	–	0.01 (.02)	0.06 (.01)	0.03 (.03)
MgO	3.14 (.16)	3.74 (.08)	4.78 (.07)	1.54 (.25)	1.81 (.11)	1.85 (.17)
CaO	8.79 (.21)	8.98 (.18)	8.44 (.11)	6.77 (.55)	6.73 (.12)	5.86 (.14)
Na_2O	3.59 (.08)	3.23 (.05)	3.52 (.09)	3.62 (.43)	3.69 (.45)	4.28 (.10)
K_2O	0.69 (.07)	0.56 (.06)	0.69 (.05)	1.05 (.20)	1.02 (.04)	1.51 (.10)
Total	99.11	98.15	97.47	101.40	99.73	99.44
FM	3.87	3.12	4.97	2.88	3.19	3.59

	T44 (7)	T50 (7)	T51 (5)
SiO_2	52.95 (.15)	46.84 (.34)	50.93 (.40)
TiO_2	7.41 (.19)	7.14 (.31)	1.67 (.12)
Al_2O_3	15.60 (.15)	14.67 (.23)	17.30 (.15)
FeO	5.89 (.13)	4.33 (.34)	3.16 (.19)
MnO	0.08 (.02)	–	–
MgO	4.54 (.10)	6.33 (.21)	2.86 (.23)
CaO	5.78 (.03)	8.91 (.22)	8.68 (.17)
Na_2O	2.74 (.03)	3.64 (.31)	3.50**
K_2O	2.08 (.08)	0.52 (.07)	.88 (.14)
Total	47.08	92.38	88.98
FM	6.52	6.52	3.75

TABLE 3

Compositions referred to in this study

	A	B	C	D	E	F	G	H	I	J	K
P(Kb)	30	30	30	30	30	33	32	31	29.8	28.5	25
T°C	900	1000	1100	1200	1400	1435	1431	1427	1421	1416	1402
SiO_2	62.3	48.8	48.1	48.4	59.64	54.41	52.92	5.192	51.21	50.68	50.26
TiO_2	–	–	–	–	–	2.17	1.95	1.80	1.70	1.62	1.56
Al_2O_3	22.7	25.0	21.1	18.5	17.67	16.28	16.6	16.82	16.97	17.09	17.18
FeO	2.3	8.4	10.1	10.3	6.25	8.33	8.45	8.53	8.59	8.64	8.67
MnO	–	–	–	–	.07	.19	.18	.18	.17	.17	.17
MgO	–	2.9	4.9	6.4	2.24	1.79	3.62	4.84	5.71	6.37	6.87
CaO	7.9	11.7	13.1	14.1	8.78	11.25	11.45	11.59	11.68	11.76	11.81
N_2O	3.6	2.5	2.2	1.9	2.82	4.28	3.77	3.43	3.19	3.01	7.87
K_2O	0.7	0.3	0.2	0.1	.87	.4	.32	.27	.23	.2	.18
P_2O_5	–	–	–	–	–	.4	.32	.27	.23	.2	.18
FM	1.69	3.96	5.75	7.15	3.59	5.29	5.88	6.28	6.58	6.81	6.99
F	0.2	0.4	0.6	0.8	.33	.4	.5	.6	.7	.8	.9
Ti_{sat}	.51	1.51	3.72	7.81	7.06	11.02	12.61	13.83	14.74	15.61	16.25

A, B, C, D — Calculated liquid compositions for partial melting of a gabbro with 5 wt% H_2O (from Stern and Wyllie, 1978, Table 8).

E — Experimentally determined liquid composition from a Hi-Al basalt equilibrated at 30 Kb 1400°C (Johnston, 1986).

G–K — Liquid compositions calculated by subtracting a crystalline assemblage of .383 Gt and .617 Cpx from a basalt along the intermediate ascent curve ofr Brophy and Marsh (1986). The mineral compositions were those determined by Green and Ringwood (1968) for a Hi-Al quartz tholeiite at 36 Kb, 1490°C (Table 10).

Fig 1

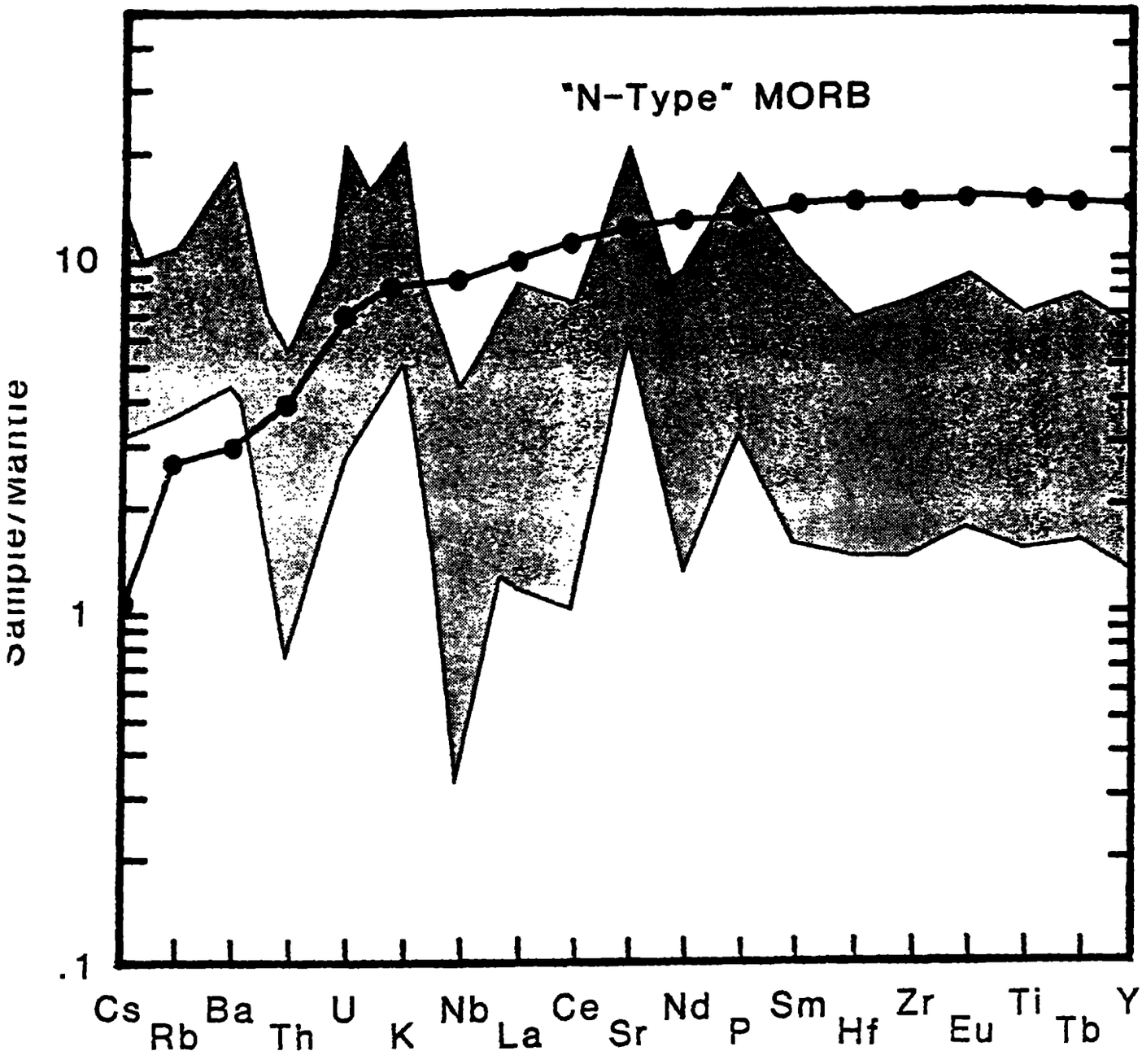
"N-Type" MORB
10
1
.1
Sample/Mantle
Cs
Rb
Ba
Th
U
K
Nb
La
Ce
Sr
Nd
P
Sm
Hf
Zr
Eu
Ti
Tb
Y

Fig. 2

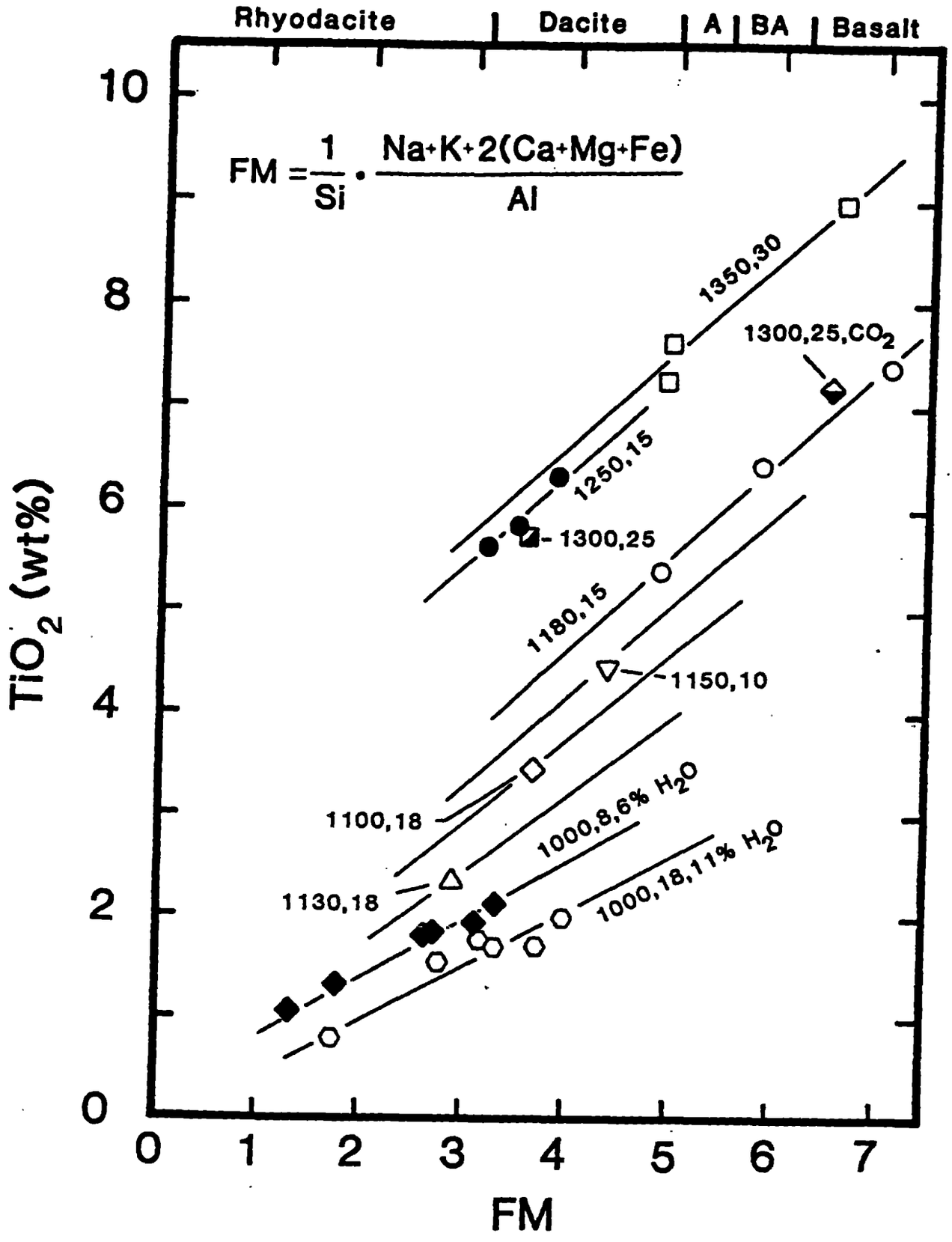
Rhyodacite
Dacite
A
BA
Basalt
$FM = \frac{1}{Si} \cdot \frac{Na+K+2(Ca+Mg+Fe)}{Al}$
1350,30
1300,25,CO_2
1250,15
1300,25
1180,15
1150,10
1100,18
1000,8,6% H_2O
1130,18
1000,18,11% H_2O
TiO_2 (wt%)
FM
0
1
2
3
4
5
6
7
0
2
4
6
8
10

Fig 3

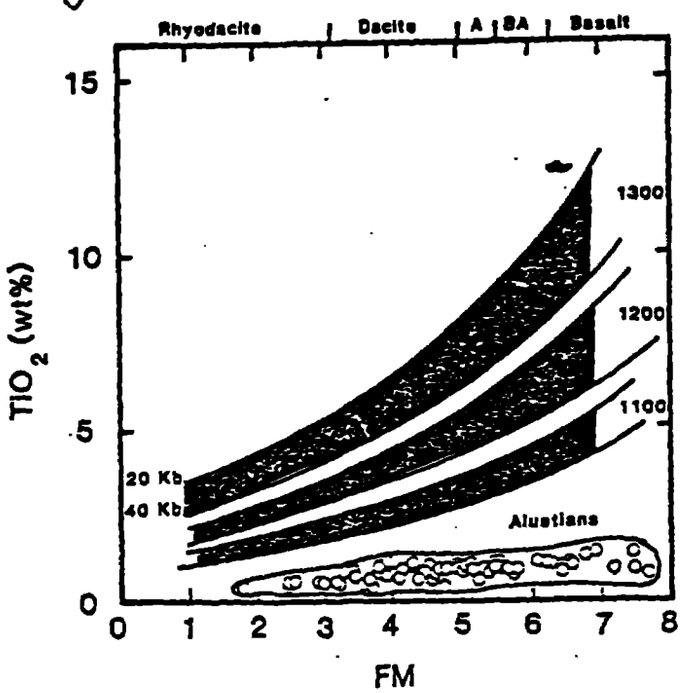
Rhyodacite
Dacite
A
BA
Basalt
15
10
5
0
TiO_2 (wt%)
1300
1200
1100
20 Kb
40 Kb
Aluetians
0 1 2 3 4 5 6 7 8
FM

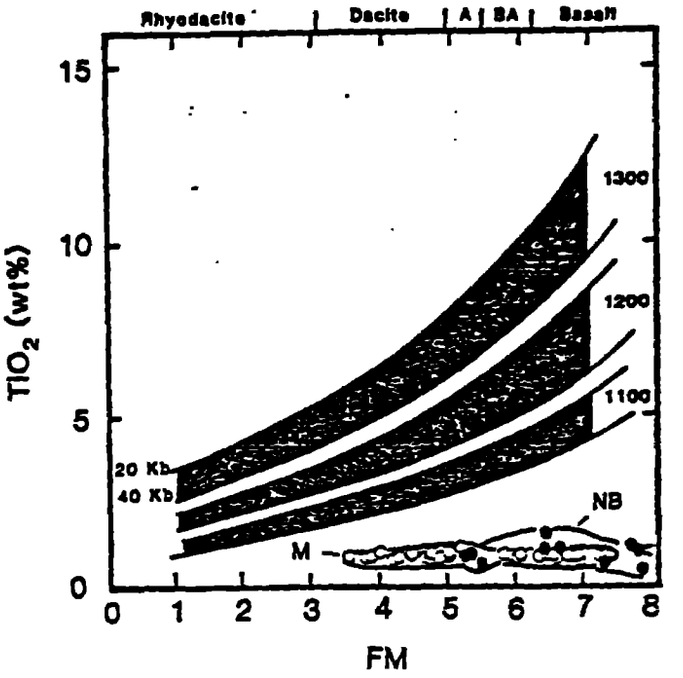
Rhyodacite
Dacite
A
BA
Basalt
15
10
5
0
TiO_2 (wt%)
1300
1200
1100
20 Kb
40 Kb
NB
M
0 1 2 3 4 5 6 7 8
FM

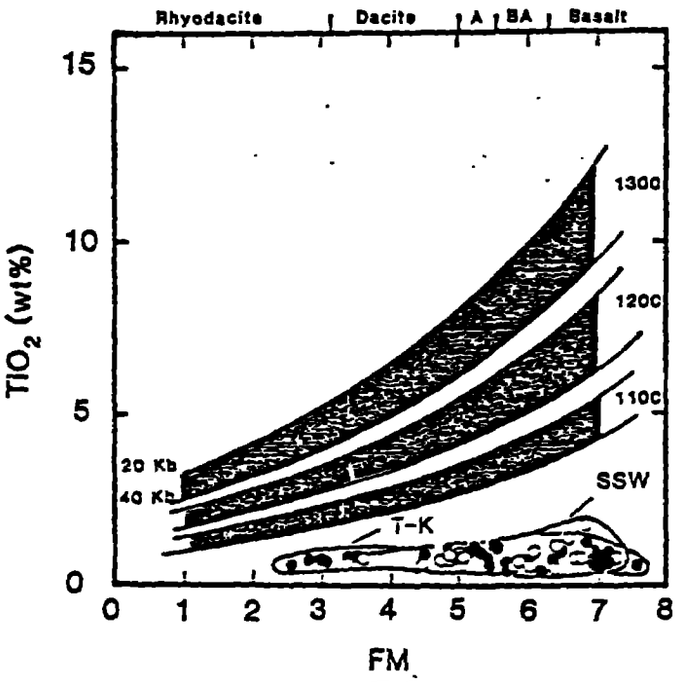
Rhyodacite
Dacite
A
BA
Basalt
15
10
5
0
TiO_2 (wt%)
1300
1200
1100
20 Kb
40 Kb
SSW
T-K
0 1 2 3 4 5 6 7 8
FM

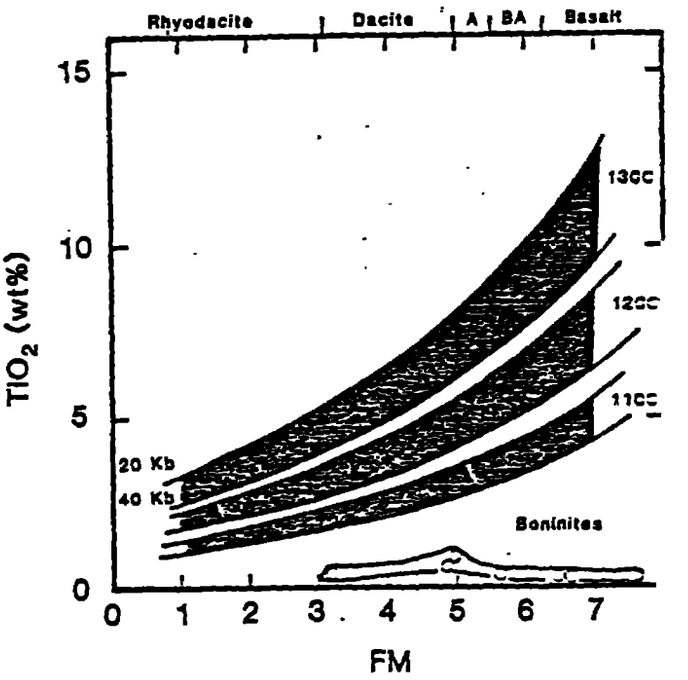
Rhyodacite
Dacite
A
BA
Basalt
15
10
5
0
TiO_2 (wt%)
1300
20 Kb
40 Kb
Boninites
0 1 2 3 4 5 6 7
FM

Fig 4

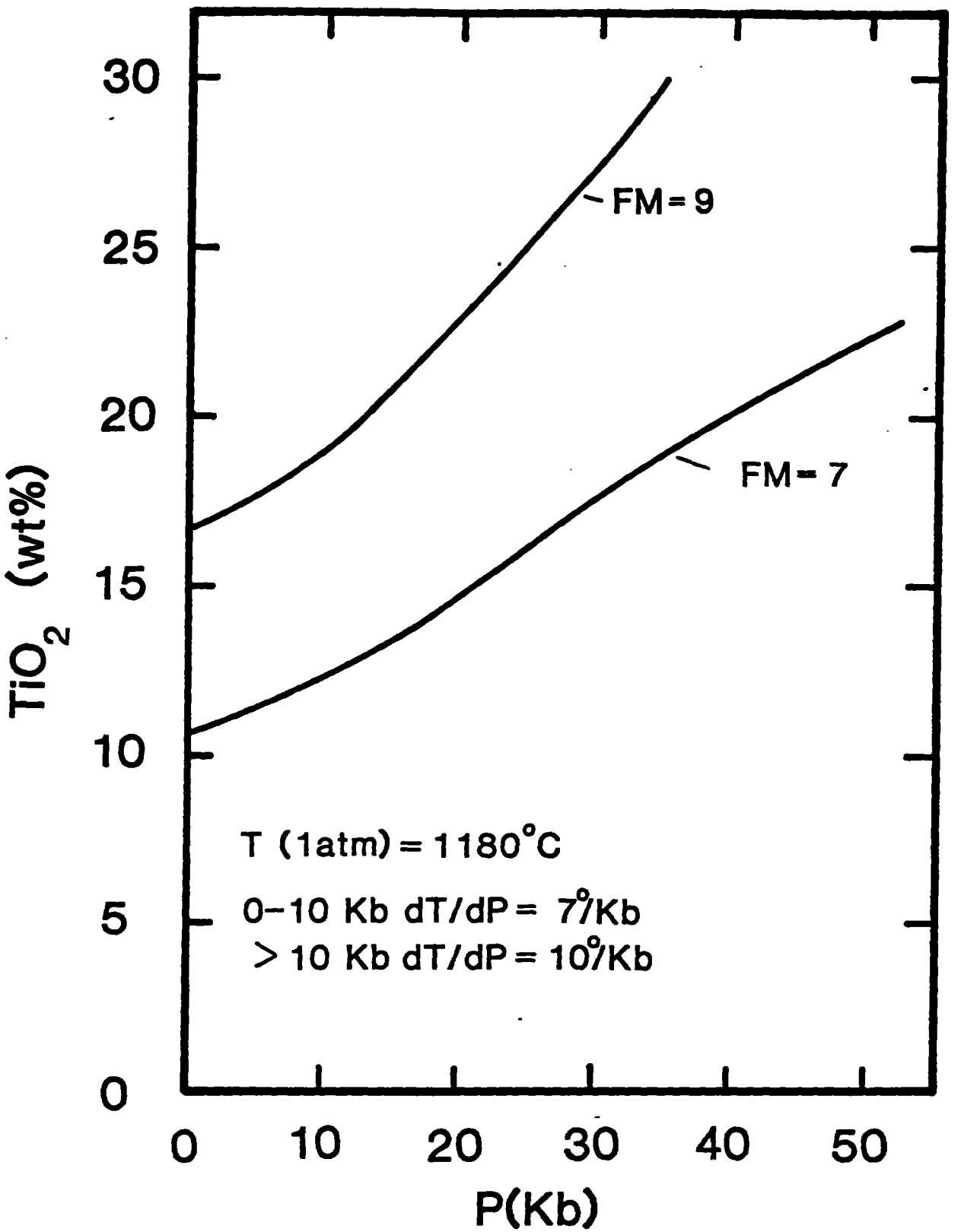

Figure 4

Figure 5

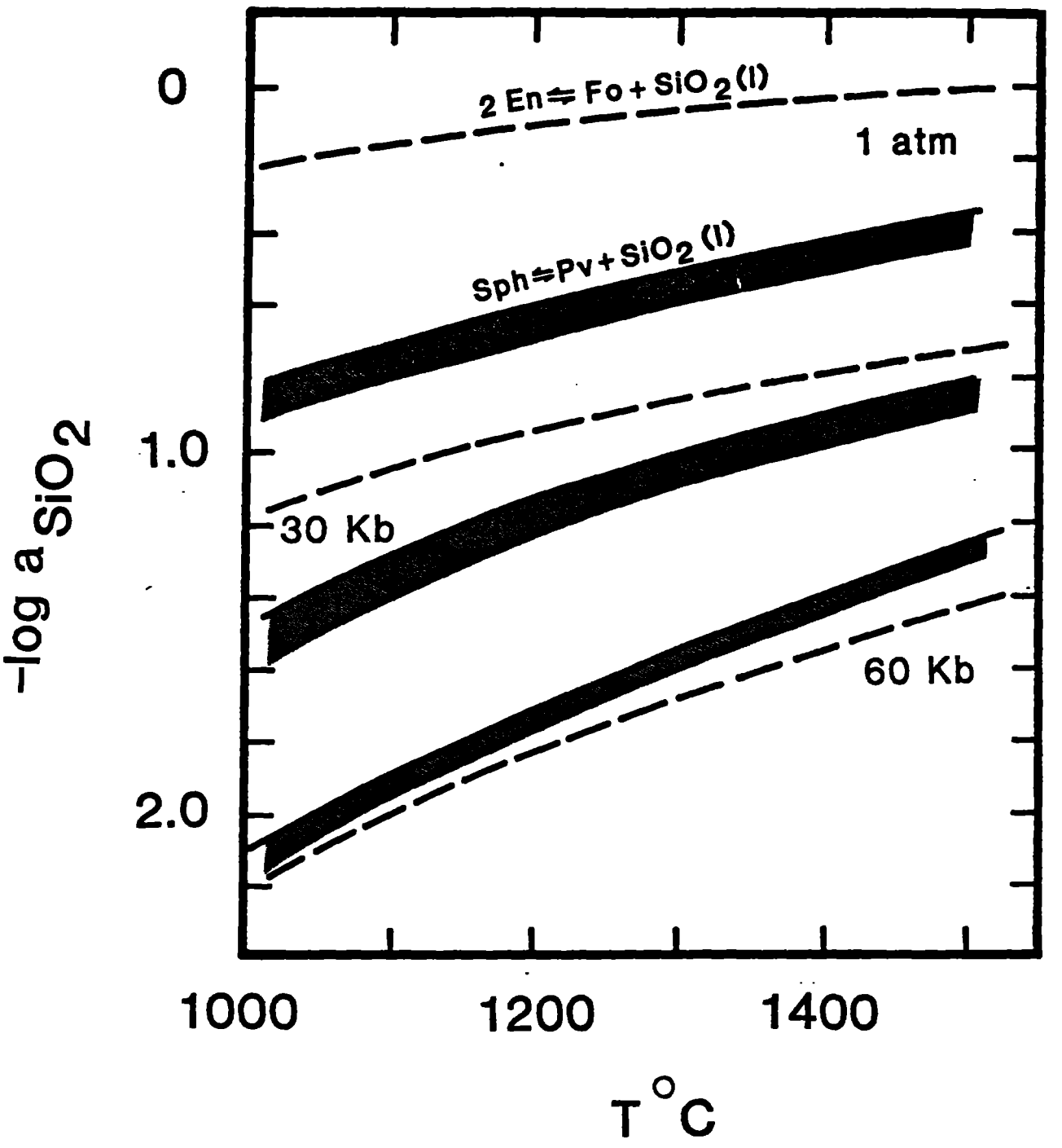

Figure 5

Fig 6a

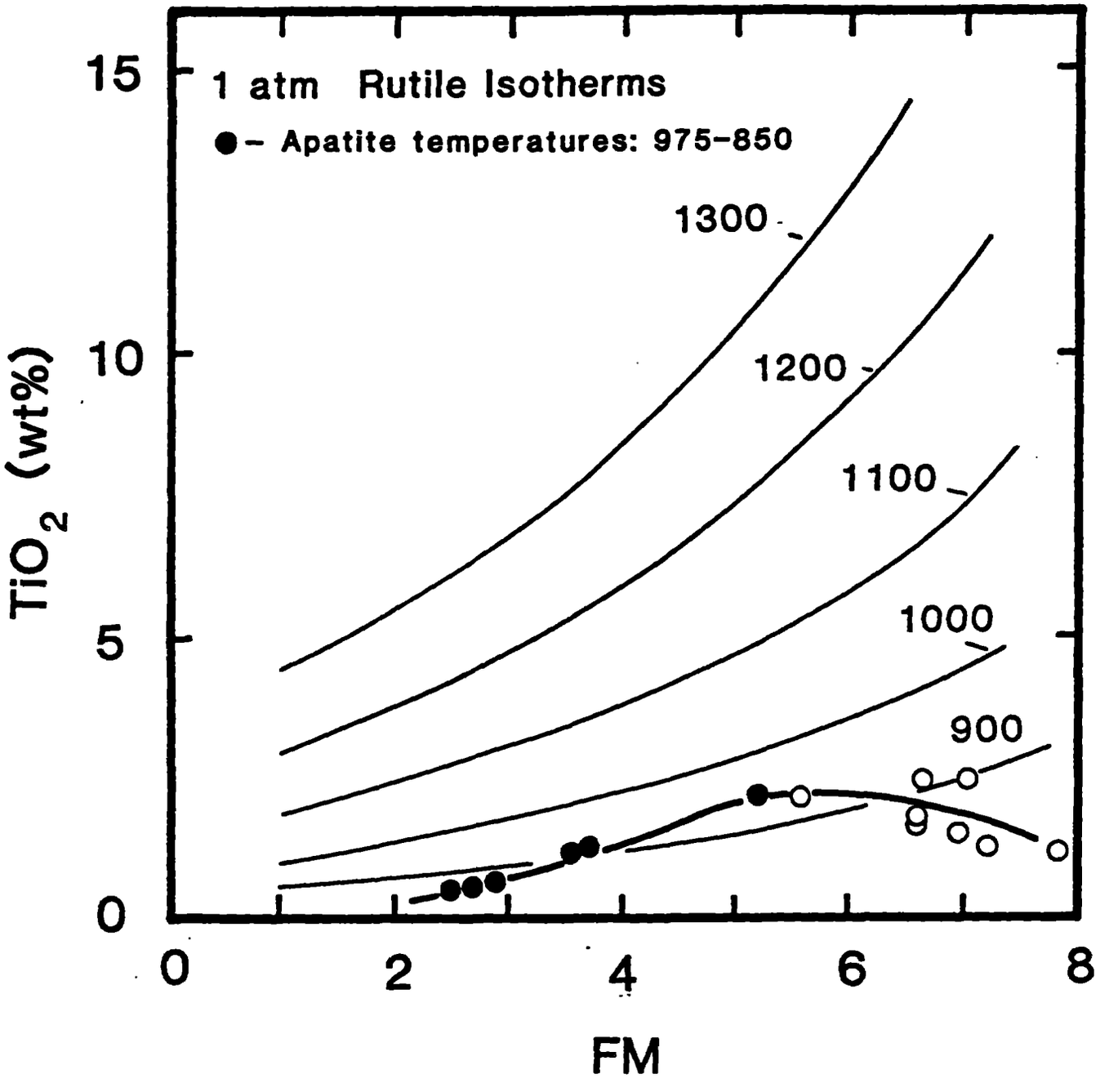
1 atm Rutile Isotherms
● – Apatite temperatures: 975–850
1300
1200
1100
1000
900
TiO2 (wt%)
FM
0
5
10
15
0
2
4
6
8

Fig 6a

Fig 6b

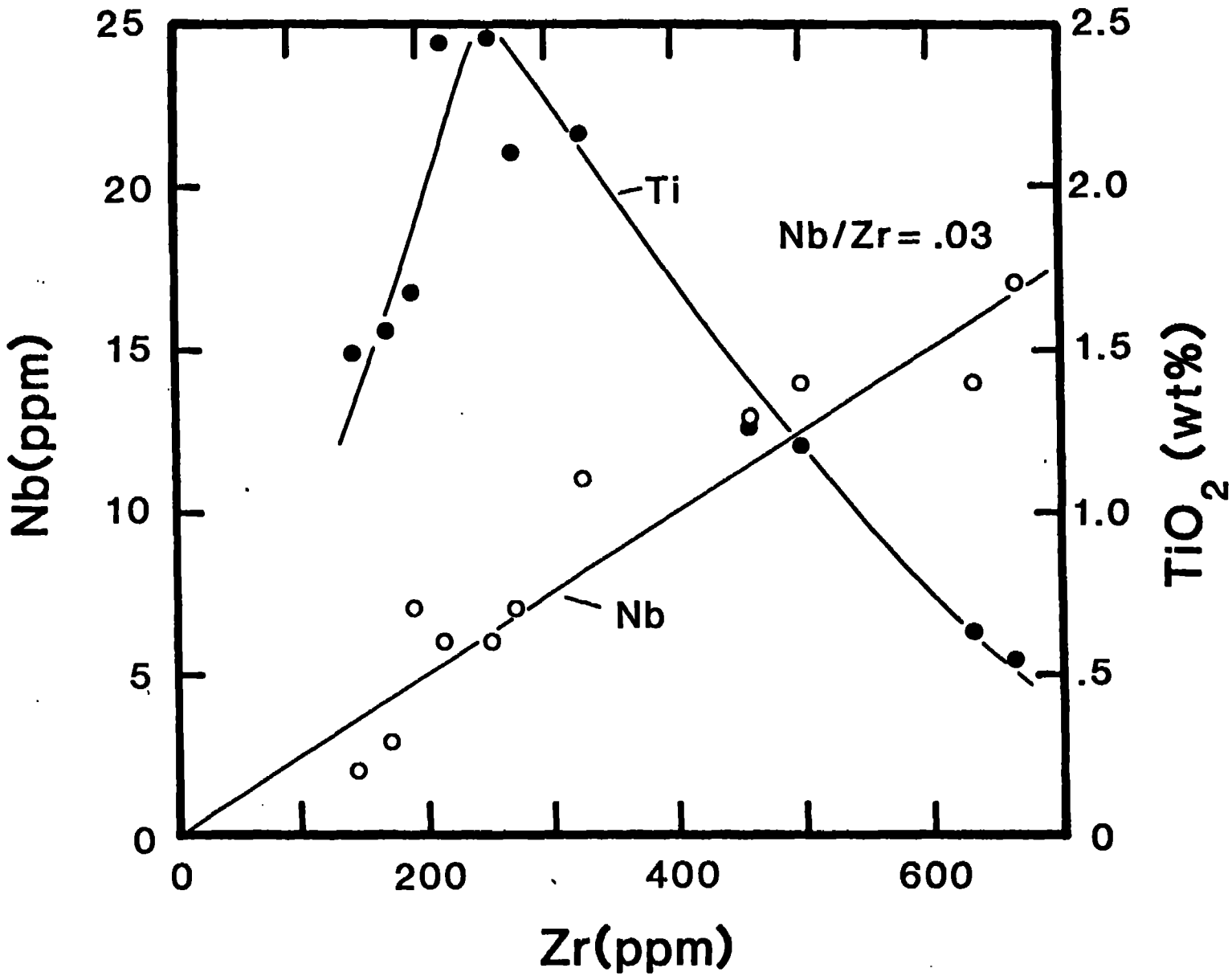
25
20
15
10
5
0
2.5
2.0
1.5
1.0
.5
0
0
200
400
600
Nb(ppm)
TiO2 (wt%)
Zr(ppm)
Ti
Nb/Zr = .03
Nb

Fig. 7a

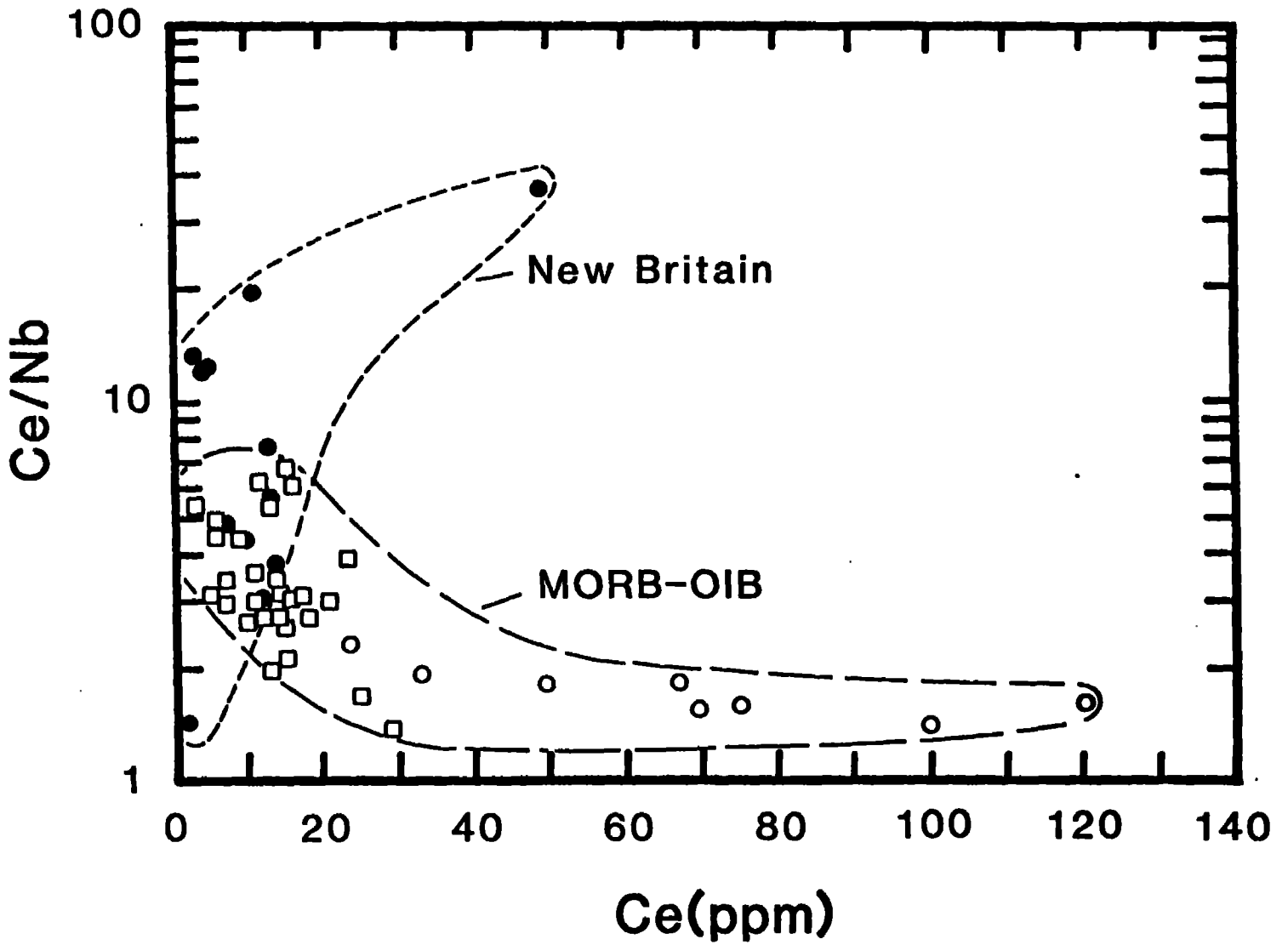
100
10
1
Ce/Nb
New Britain
MORB-OIB
0
20
40
60
80
100
120
140
Ce(ppm)

Fig 7b

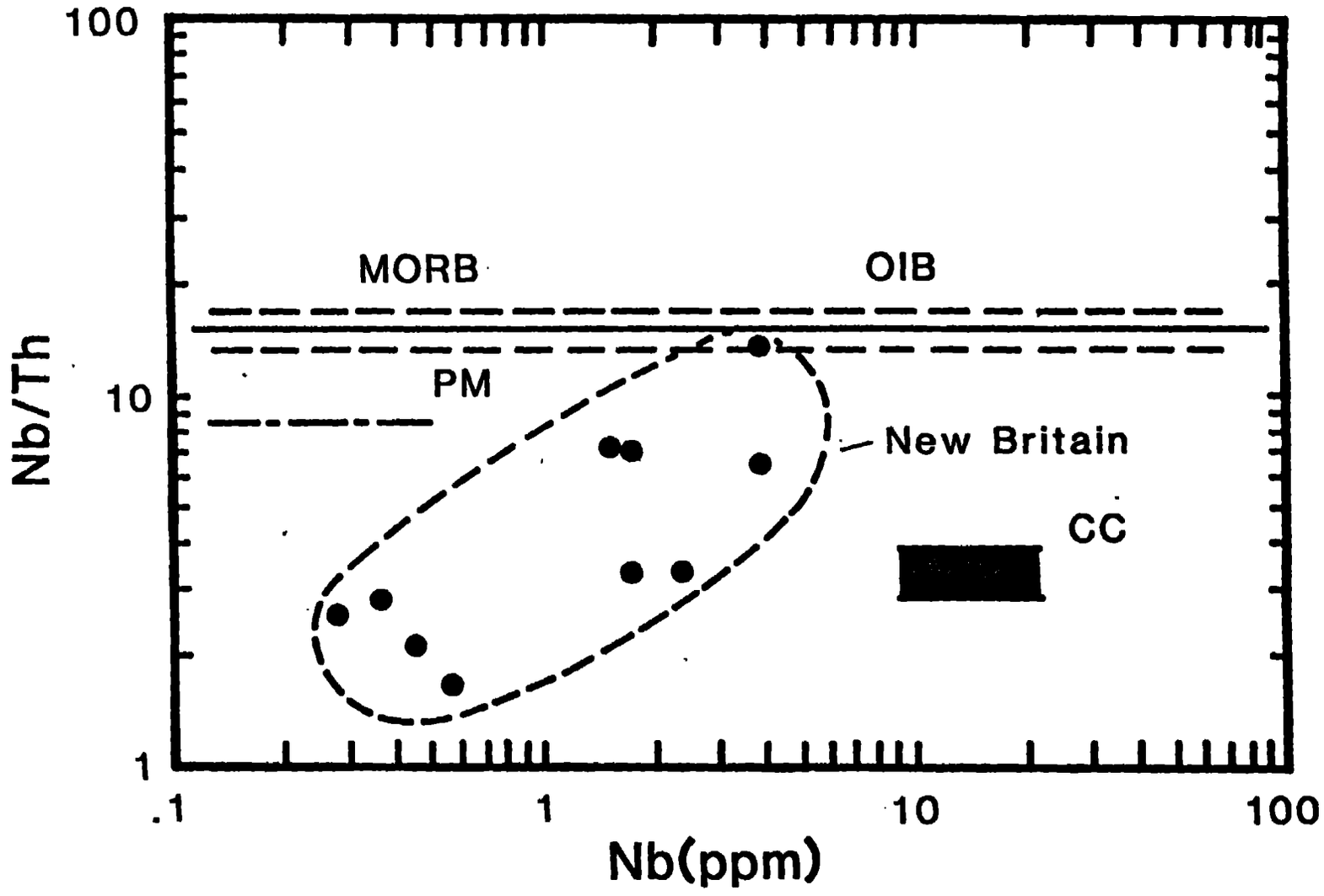

Fig 8

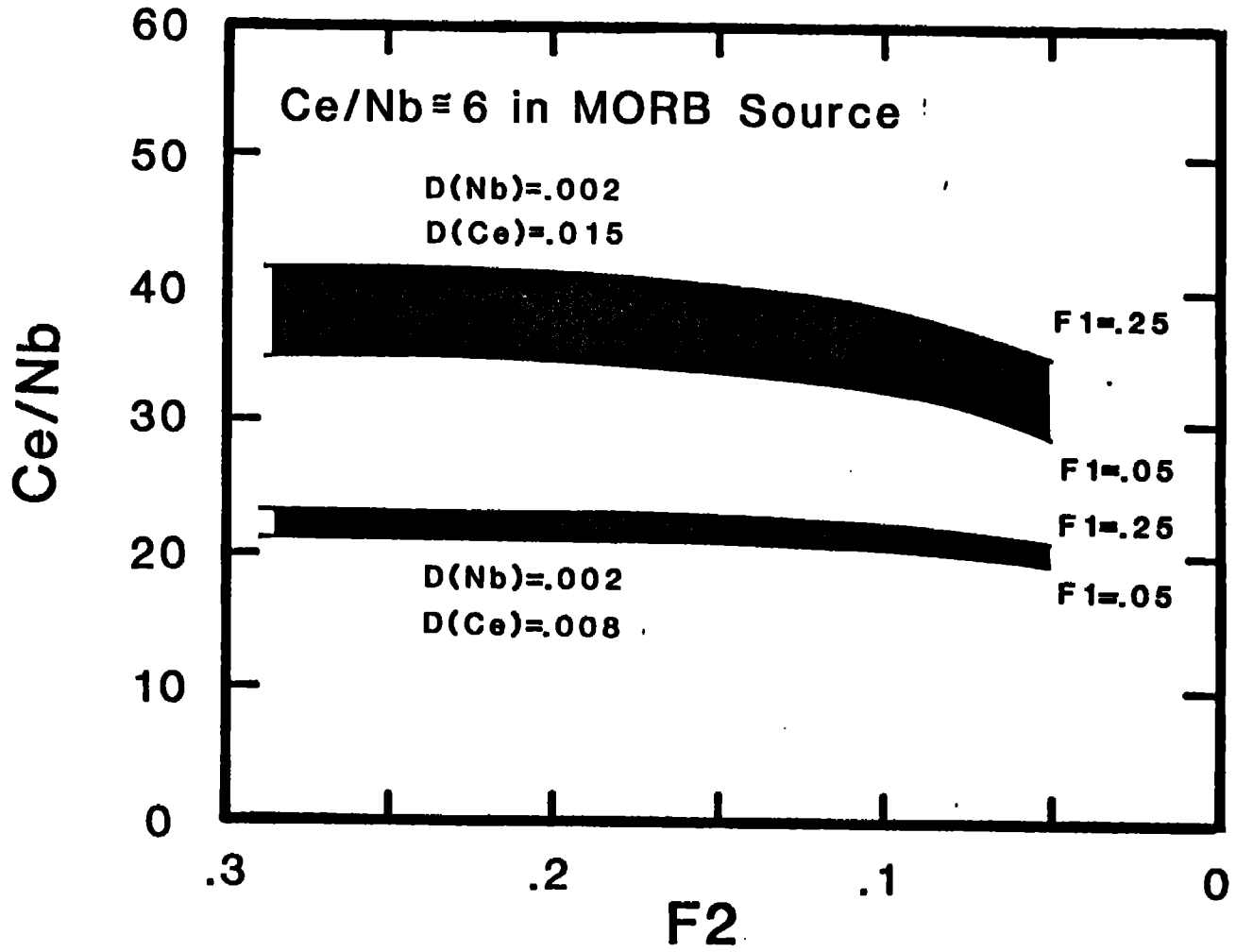
Ce/Nb ≅ 6 in MORB Source
D(Nb)=.002
D(Ce)=.015
F1=.25
F1=.05
F1=.25
F1=.05
D(Nb)=.002
D(Ce)=.008
Ce/Nb
60
50
40
30
20
10
0
.3
.2
.1
0
F2

Fig. 9